Heavy Oil

Controlled Document

Quest CCS Project

Project	Quest CCS Project
Document Title	Radway SCL 08-19-59-20W4 Basal Cambrian Sands Geomechanical Test Results
Document Number	07-3-ZG-7180-0030
Document Revision	01
Document Status	Final Report
Document Type	ZW7180-Other Report
Owner / Author	J.W.Dudley, L.A.Hathon, M.M.Arasteh
Issue Date	2011-12-16
Expiry Date	None
ECCN	EAR 99
Security Classification	Restricted
Disclosure	None

Revision History shown on next page

Revision History

REVISION STATUS			APPROVAL		
Rev.	Date	Description	Originator	Reviewer	Approver
1	2011-12-16	Final report	J.W.Dudley	S.J.Bourne, R.E.Meij	S.Crouch
• All signed originals will be retained by the UA Document Control Center and an electronic copy will be stored in Livelink					

Signatures for this revision

Date	Role	Name	Signature or electronic reference (email)
12/15/2011	Originator	J.W.Dudley	John.w.dudley@shell.com
	Reviewer	S.J.Bourne, R.E.Meij	Stephen.bourne@shell.com; Robert.meij@shell.com
	Approver	S.Crouch	S.Crouch@shell.com

Summary

The report documents petrology and geomechanical tests on Basal Cambrian Sand core from three zones in the Shell Canada Radway well SCL 08-19-59-20W4.

Keywords

Quest, geomechanics, BCS, strength, compressibility, TWC, UCS, friction angle, cohesion, Biot coefficient, thermal expansion coefficient, petrology

DCAF Authorities

Date	Role	Name	Signature or electronic reference (email)
		Add name	Actual signature
		Add name	Actual signature
		Add name	Actual signature

TABLE OF CONTENTS

Executive Summary

The report documents petrology and geomechanical tests on Basal Cambrian Sand core from three zones in the Shell Canada Radway well SCL 08-19-59-20W4. Suites of triaxial compression strength tests provide loading Young's modulus (YM), Poisson's ratio, friction angle and cohesion measurements. Uniaxial constant-lateral-strain pore pressure inflation-depletion tests provide uniaxial compaction coefficient C_m and pore volume compressibility C_p measurements appropriate for estimating reservoir and surface deformations, and reservoir pore volume change behaviours. Isotropic bulk volume compressibility C_b tests provide bulk and pore volume change behaviour under an isotropic compression stress path. The uniaxial strain and isotropic compression tests also provide estimates of the formation Biot coefficient. Detailed digital test data, results and petrographic images are included in an accompanying data DVD.

The different measurements under different stress paths provide a range of mechanical parameters for the BCS formation. Although the compressibility measurements show a marked non-linear increase as the rocks approach zero effective stress, unstressed thin section analysis indicates this behaviour may be related to sample disturbance. For base case modeling considerations we recommend using constant compressibility values estimated from the data ranging from a few MPa below initial in-situ effective stress conditions to full depletion conditions (i.e., pore pressure range 0-25 MPa).

The ranges of the various geomechanical parameter values measured are given in the table below, together with a self-consistent set of linear poro-thermo-elastic parameters for the reservoir material tested. The set is based primarily on the uniaxial-strain tests, which are the closest stress path to likely field operations. Although one set of parameters is given, any reservoir or geomechanical simulations or calculations done using these values should also include significant parameter sensitivity calculations to cover at least the full range of behaviour seen in these tests.

Symbol	Value	Units	Measured Range Across Tests	Parameter Description
Cmp	0.036	1/GPa	0.027 - 0.041	Uniaxial compaction coefficient under depletion
Cpp	0.38	1/GPa	0.24 - 0.49	Uniaxial pore volume compressibility under depletion
γ	0.69	--	0.65 - 0.77	Horizontal depletion constant
α_B	0.80	--	0.63 - 0.78	Biot coefficient
ν	0.12	--	0.15 - 0.36	Poisson's ratio from α, γ
E	21.33	GPa	15.1 - 29.5	Young's Modulus from Cmp, ν, γ
G	9.54	GPa	6.3 - 10.8	Shear modulus from E, ν
K(elas)	9.30	GPa	7.3 - 36.2	Drained bulk modulus from E, ν
Ks	46.48	GPa	21.9 - 34.3	Grain modulus from α, K
θ	41.3	fractional	37.2 - 44.4	Friction Angle
c	10.3	MPa	9.4 - 12.5	Apparent cohesion
α_T	1.03E-05	1/C	0.99e-5 - 1.07e-5	Linear thermal expansion coefficient

1. INTRODUCTION

This report documents geomechanical measurements made on Basal Cambrian Sands (BCS) core material from well Radway SCL 08-19-59-20W4. These measurements are in support of Shell Canada's participation in the Quest carbon dioxide (CO_2) sequestration project. The measurements are addressed at quantifying the strength and deformation behaviour of the target CO_2 injection reservoir related to sand failure and pore volume changes. A short introduction to the stratigraphy and petrology is presented next, followed by sections describing the compressive strength, volume compressibility, and thermal expansion behaviours, respectively. The report concludes with a summary discussion of the results and advice on a geomechanical parameter suite for the BCS. Detailed digital data and images are included in an accompanying DVD.

1.1. Quest Stratigraphy

Location of the Radway 8-19 well within the Quest Area of interest is shown in **Figure 1-1**(El Mahdy, et al, 2011). This well is currently intended to be used as a CO_2 injection well. A schematic stratigraphy of the relevant formations is provided in **Figure 1-2**(El Mahdy, et al, 2011). Core was recovered from the lower four formations shown in the stratigraphy diagram from the Radway 8-19 well. This report only presents geomechanical testing results on the BCS material.

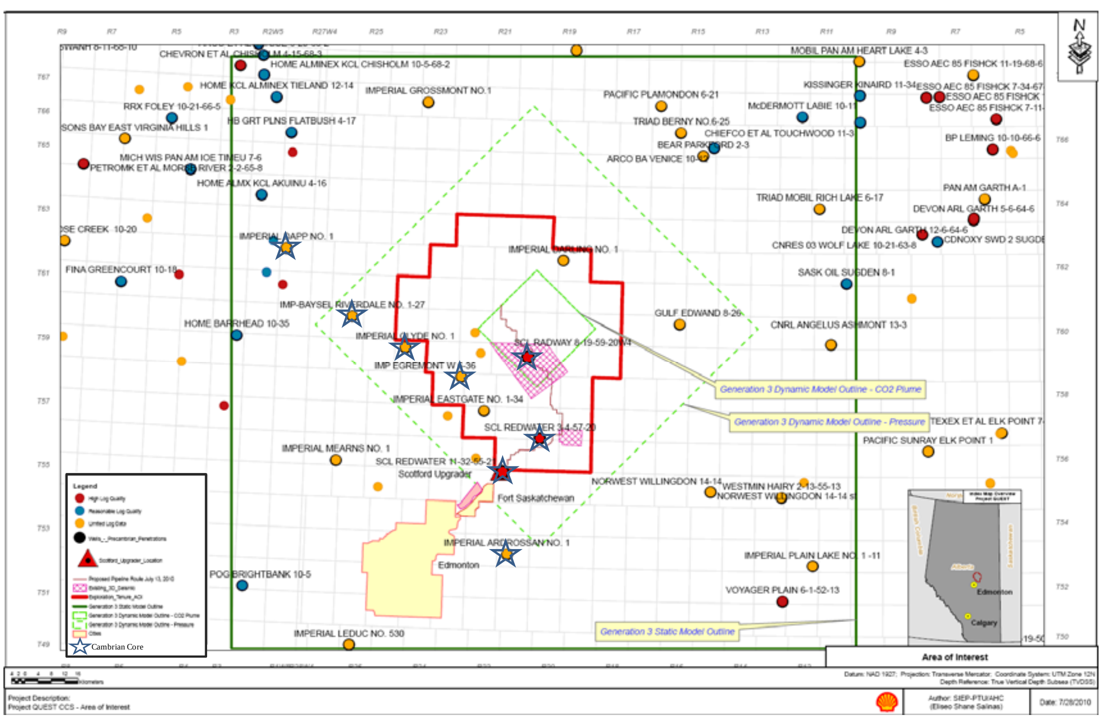

Figure 1-1. Radway 8-19 location in the centre of the Quest Area of Interest (red contour) superimposed with legacy well penetrations (from El Mahdy, et al, 2011).

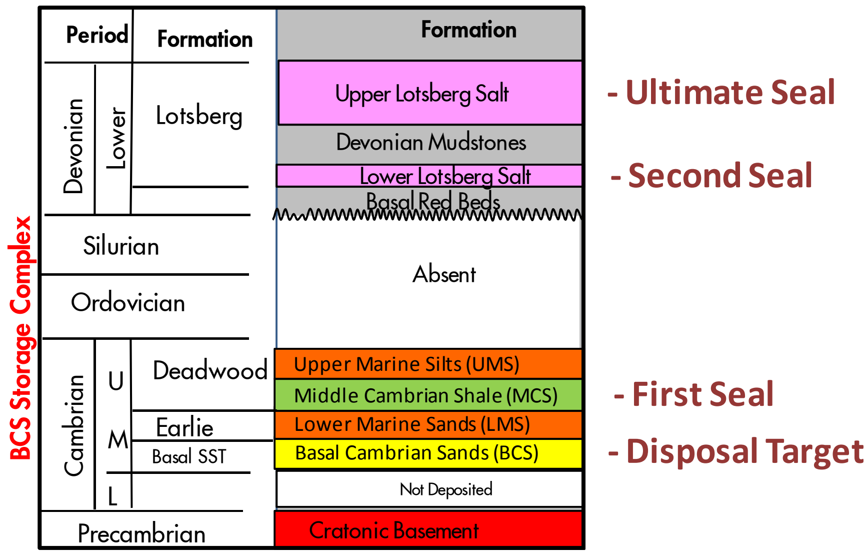

Figure 1-2. Schematic diagram of the relevant formation stratigraphy of the Radway 8-19 well (from El Mahdy, et al, 2011).

1.2. BCS petrology

Three distinct facies were identified for testing based on examination of the supplied core material. Characteristic thin sections from these three zones are shown in **Figure 1-3**, and identified by the approximate core depth of the samples tested. In-situ measured porosities on samples from the three zones were spread over the range 8 to 21 percent. A more detailed description is provided in Appendix 1.

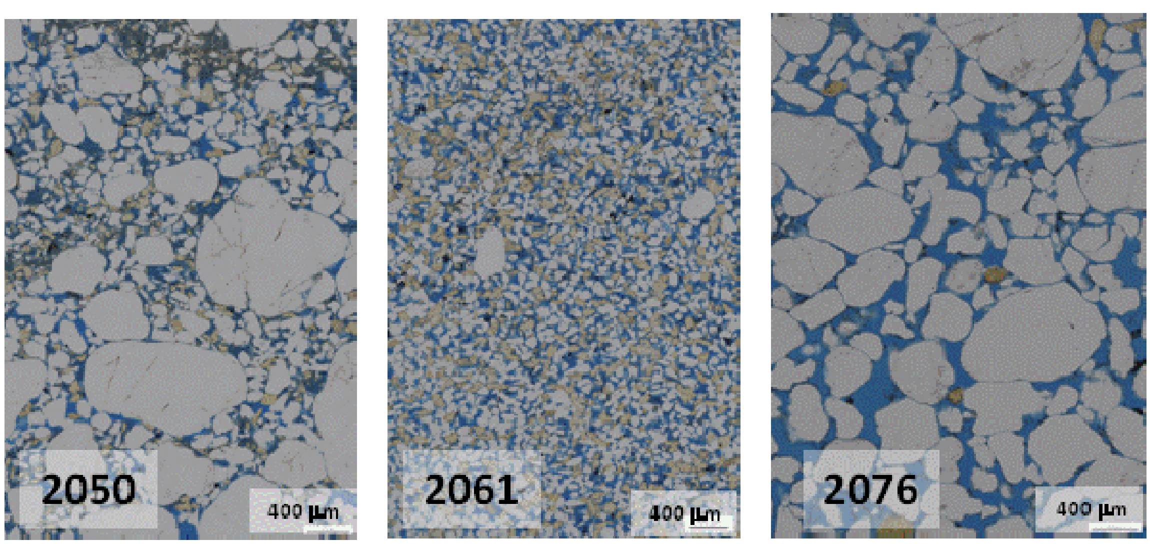

Figure 1-3. Thin section micrographs of the three BCS depth zones (in metres) identified for testing.

2. BCS STRENGTH MEASUREMENTS

This section describes the various strength measurements made on the three BCS zones identified for testing. Conventional triaxial compression, unconfined compressive strength (UCS) and thick wall cylinder collapse strength (TWC) tests are included here. A summary of all samples tested and reported is given in Table 2-1. An overview of the testing protocols is presented first, followed by a summary of the test results.

Table 2-1. Sample information summary.

Sample Name	Set	Sample Depth (m)	Sample Length (mm)	Sample Diameter (mm)	Test Type	As-Received Weight (g)	Dry, Cleaned Weight (g)	Bulk Density (g/cc)	Porosity in-situ cond. (%)	Grain Density (g/cc)
RAD002	1	2076.25	51.23	25.27	1.0X Triax	54.89	--	2.133	--	--
RAD003		2076.25	50.52	25.27	1.5X Triax	54.53	--	2.149	--	--
RAD006A		2076.25	42.47	25.32	Uniax-ppid	--	43.18	2.016	21.26	2.608
RAD031		2076.39	45.31	25.58	UCS	54.82	--	2.351	--	--
RAD033		2076.39	36.40	25.43	Isostatic	--	40.46	2.186	12.86	2.488
RAD037		2076.39	50.55	25.40	0.5X Triax	58.18	--	2.268	--	--
RAD032		2076.39	52.86	25.40	TWC	56.32	--	2.100	--	--
RAD004		2076.25	*	*	Texp	*	--	*	--	--
RAD034		2076.39	*	*	Texp	*	--	*	--	--
RAD043	2	2050.19	50.83	25.45	Isostatic	--	60.36	2.331	8.22	2.580
RAD052		2050.39	48.62	25.50	0.5X Triax	61.50	--	2.473	--	--
RAD054		2050.39	51.05	25.48	1.0X Triax	61.52	--	2.361	--	--
RAD055		2050.39	50.85	25.55	Uniax-ppid	--	60.52	2.318	11.41	2.655
RAD056		2050.39	50.77	25.53	UCS	61.32	--	2.357	--	--
RAD058		2050.39	50.09	25.48	1.5X Triax	59.95	--	2.345	--	--
RAD051		2050.32	46.43	25.40	TWC, Texp	51.26#	--	2.451	--	--
RAD053		2050.32	*	*	Texp	*	--	*	--	--
RAD072	3	2060.79	38.35	25.53	Isostatic	--	40.02	2.036	18.76	2.536
RAD073		2060.79	50.32	25.50	1.5X Triax	59.94	--	2.329	--	--
RAD074		2060.79	31.50	25.50	Uniax-ppid	--	34.74	2.157	12.29	2.509
RAD076		2060.79	51.10	25.48	0.5X Triax	60.68	--	2.326	--	--
RAD077		2060.79	49.45	25.50	UCS	59.90	--	2.368	--	--
RAD078		2060.79	44.91	25.50	1.0X Triax	52.78	--	2.298	--	--
RAD091		2060.89	45.77	25.40	Texp	66.63	--	2.868	--	--

* Samples for not yet completed thermal expansion measurements; data will updated when testing completed;
# Weight after 8-mm borehole drilled;
Test Type codes: UCS – unconfined compressive strength; TWC – thick wall cylinder collapse strength; Isostatic – isotropic compression; Uniax-ppid – uniaxial strain pore pressure inflation-deflation; #X Triax – triaxial compressive strength test at #*21.3MPa confining stress; Texp – linear thermal expansion

2.1. Testing Protocols

All tests are conducted on a convention triaxial testing apparatus with independent axial, confining, and pore pressure control systems. PC-based software performs all data acquisition and control. The strength tests are conducted on ‘as received’ samples without prior cleaning. Samples are inserted into the test vessel, a nominal confining pressure is applied (1-2 MPa), and then saturated with the synthetic brine (200 ppm NaCl). For the triaxial compression tests samples are then typically taken to the test confining pressure and left to equilibrate for 12 hours, sufficient time for sample and equipment to stabilize. Samples are then loaded at a strain rate of approximately 0.5x10^{-6}/second to failure. This rate is slow enough for the results to representative of the quasi-static conditions expected for the field loading rates. Triaxial compression tests are done at confining stresses of 10.7 MPa, 21.3 MPa and 32.0 MPa. These values represent 0.5, 1.0 and 1.5 times the estimated mean effective stress of the BCS formation in the Radway 8-19, based on stress and pore pressure information supplied by A. Simone, petrophysical engineer working with the Quest team. Table 2-2 details the stress estimation information.

Table 2-2 In-situ stress information

Sh based on minifrac closure pressure of 34.6 MPa at core depth of 2045 m:				
Sh_gradient = 34600kPa/2045m:	16.92	kPa/m, relative to core depths		
Sh at 2076 m core depth:	35.12	MPa	5094	psi
SV_gradient from GBS team:	23.43	kPa/m	1.036	psi/ft
SV at 2076 core depth:	48.65	MPa	7056	psi
Assumned SH = (SV+Sh)/2:	41.89	MPa	6075	psi
Mean Horizontal Stress (SH+Sh)/2:	38.51	MPa	5585	psi
Mean Total Stress (SV+SH+Sh)/3:	41.89	MPa	6075	psi
Radway Pore pressure (MDT) at 2076 m core depth:	20.56	MPa	2982	psi
Mean Horz. Eff. Stress (Terzaghi, S_horz.mean - Ppore):	17.95	MPa	2603	psi
Mean Effective Stress (Terzaghi, Smean - Ppore):	21.33	MPa	3093	psi

2.2. Compressive Shear Strength Test Results

The triaxial strength and UCS test results are summarized in Table 2-3. Triaxial stage stress-strain data plots for each of the test zones are provided in Figure 2-1, Figure 2-2 and Figure 2-3. The data regions over which the loading Young’s modulus Poisson’s ratio are calculated are highlighted in gray on the curves (these are not listed for the UCS (zero confining stress) tests as these are not representative of subsurface conditions). Plots showing the Mohr-Coulomb friction angle and apparent cohesion determination are given in Figure 2-4. The strength properties of the three zones are similar, with friction angles in the range 37.2 - 42.2 degrees and cohesion in the range 9.4 - 12.5 MPa. The Young’s modulus and Poisson’s ratio are more variable, and range from 15.1 - 29.5 MPa and 0.15 - 0.36, respectively. The zone at depth 2050m has the higher values. The top value in each set in Table 2-2 In-situ stress informationis the test at the estimated mean effective confining stress of 21.3 MPa, and these values are appropriate to use for the reservoir initial in-situ conditions.

Table 2-3. Summary of compressive strength test results

Sample Name	Set	Sample Depth (m)	Confining Stress (MPa)	Peak Deviatoric Stress (MPa)	Young's Modulus (GPa)	Poisson's Ratio	Calculated Shear Modulus (GPa)	Calculated Bulk Modulus (GPa)	Friction Angle (deg.)	Cohesion (MPa)
RAD002	1	2076.25	21.30	117.21	15.3	0.16	6.62	7.41	37.2	11.9
RAD003		2076.25	31.96	132.38	15.1	0.15	6.54	7.27		
RAD031		2076.39	0.00	40.68	N/A	N/A	N/A	N/A		
RAD037		2076.39	10.65	89.63	19.4	0.33	7.29	19.13		
RAD054	2	2050.32	21.30	133.83	27.0	0.34	10.09	27.78	42.2	9.4
RAD058		2050.32	31.96	166.16	29.5	0.36	10.81	36.15		
RAD056		2050.39	0.00	35.85	N/A	N/A	N/A	N/A		
RAD052		2050.32	10.65	94.80	22.8	0.31	8.70	20.00		
RAD078	3	2060.79	21.30	133.76	19.8	0.20	8.22	11.15	38.0	12.5
RAD073		2060.79	31.96	124.79	16.7	0.33	6.28	16.28		
RAD077		2060.79	0.00	40.33	N/A	N/A	N/A	N/A		
RAD076		2060.79	10.65	111.01	19.4	0.26	7.72	13.25		

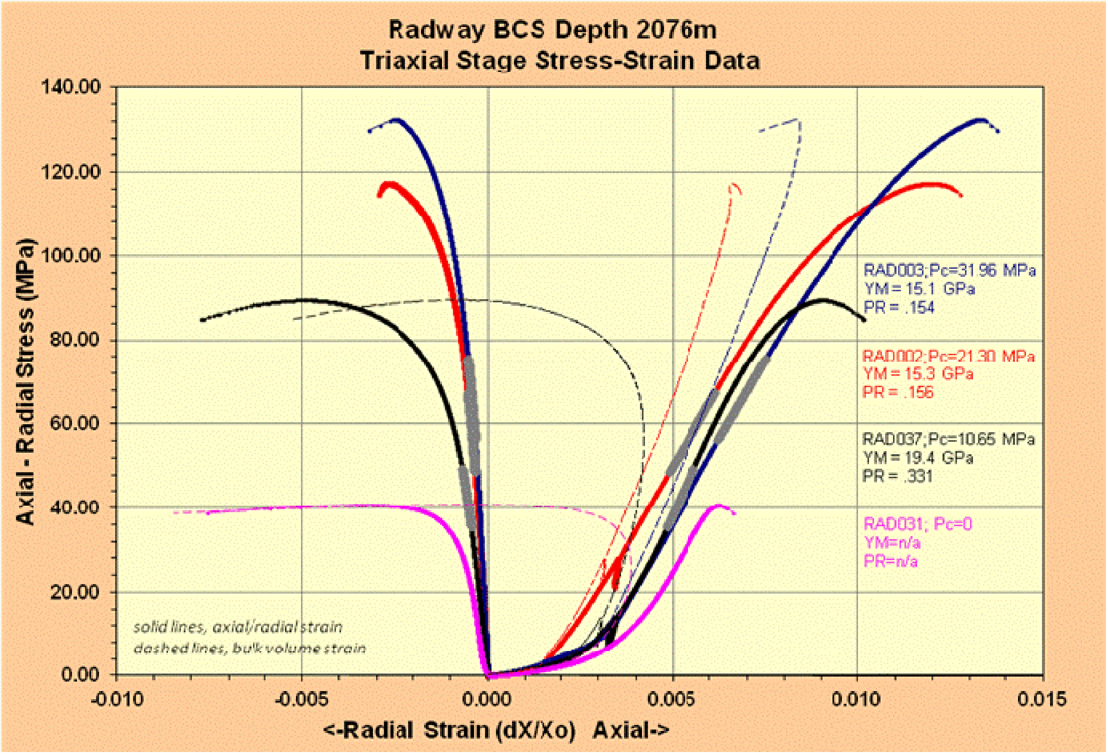

Figure 2-1. Compressive strength data from 2076 m zone.

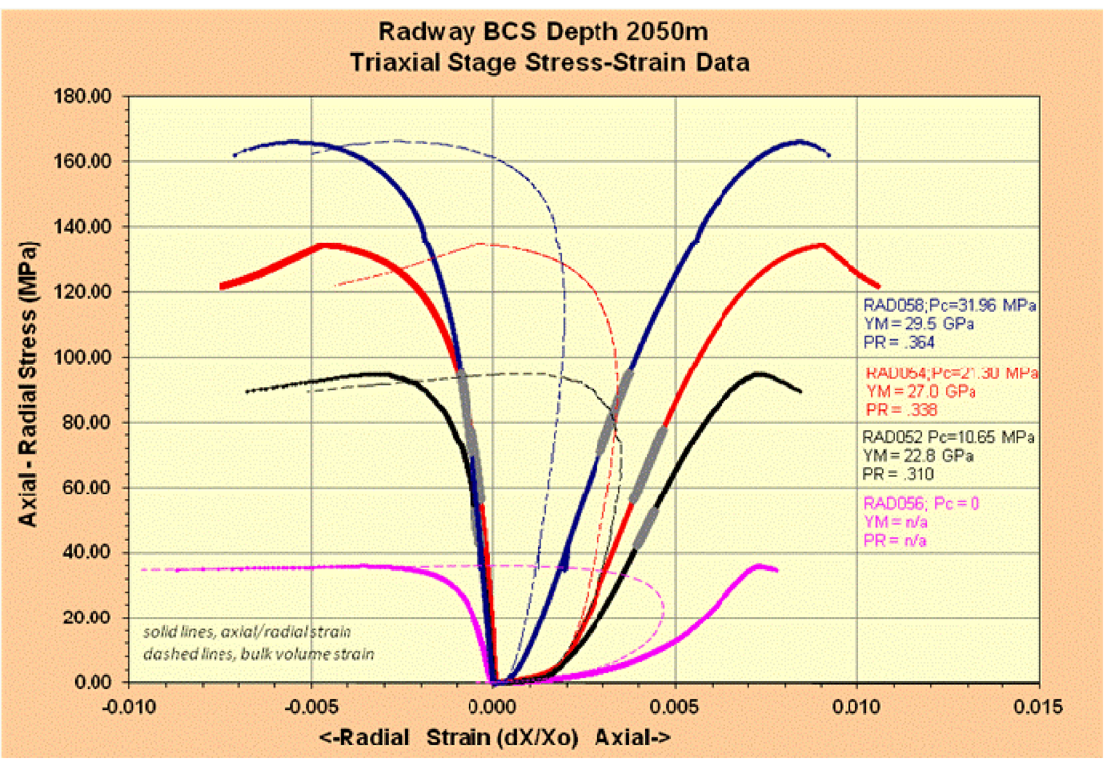

Figure 2-2. Compressive strength data from 2050 m zone.

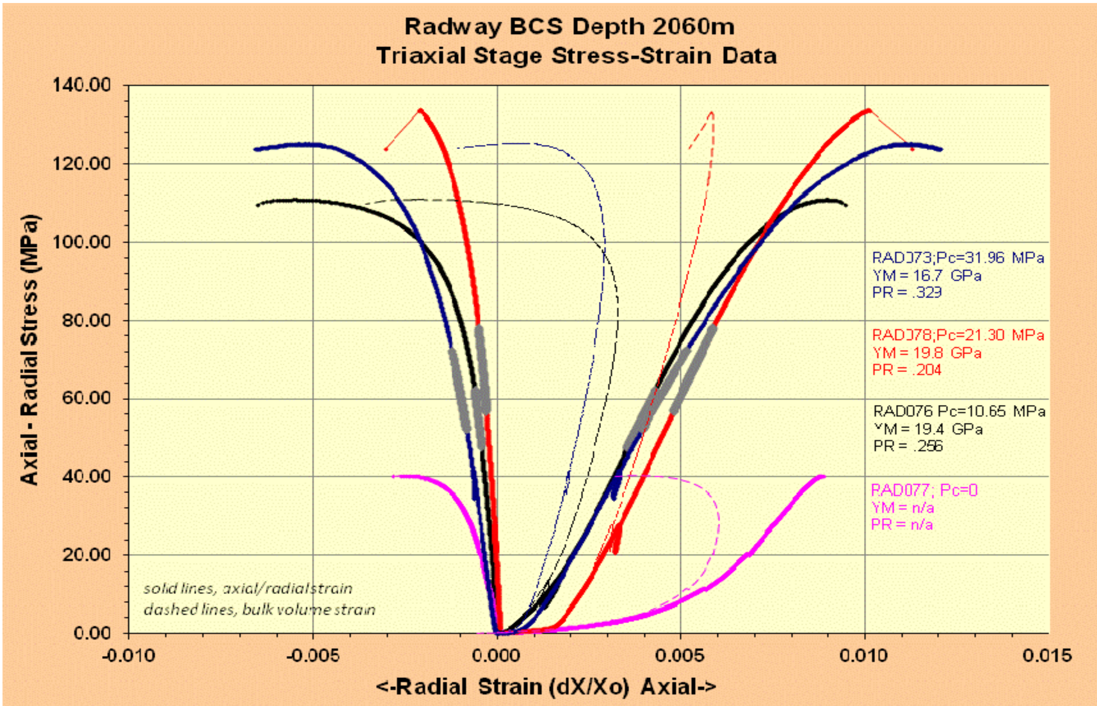

Figure 2-3.Compressive strength data from 2060 m zone.

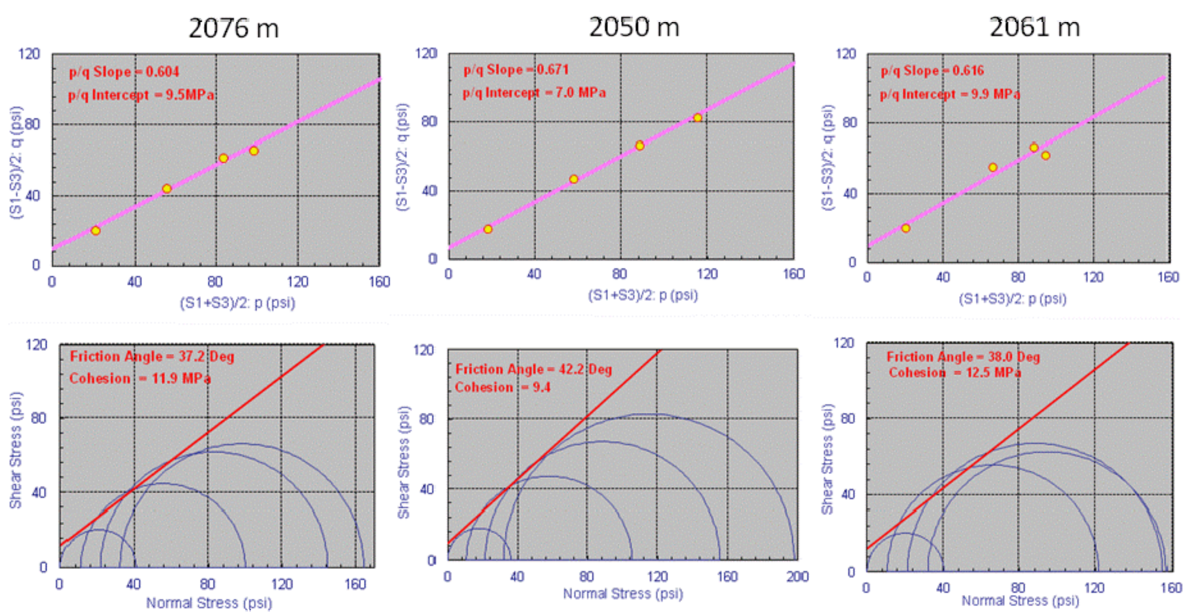

Figure 2-4. Summary of Mohr-Coulomb strength results for BCS zones tested.

2.3. Thick Wall Cylinder Collapse Strength Test Results

Only two of the zones had core samples available for TWC testing. A TWC plug was obtained from depth 2052.32 m, and pressurized to the limit of our test equipment (68.9 MPa) without failing. A TWC plug was obtained from a much weaker section at 2076.39 m, but this plug came apart while preparing it for pressure testing. Figure 2-5 summarizes these results. This plug indicates there is some friable, poorly cemented, heterogeneous rock in the BCS, which could have significantly lower UCS strength than that measured on the plugs tested. This is primarily a concern for wellbore sanding issues, rather than containment. Further testing would be required to determine a correlation between the TWC strength and log properties for making sanding predictions related to near-wellbore pressure fluctuations.

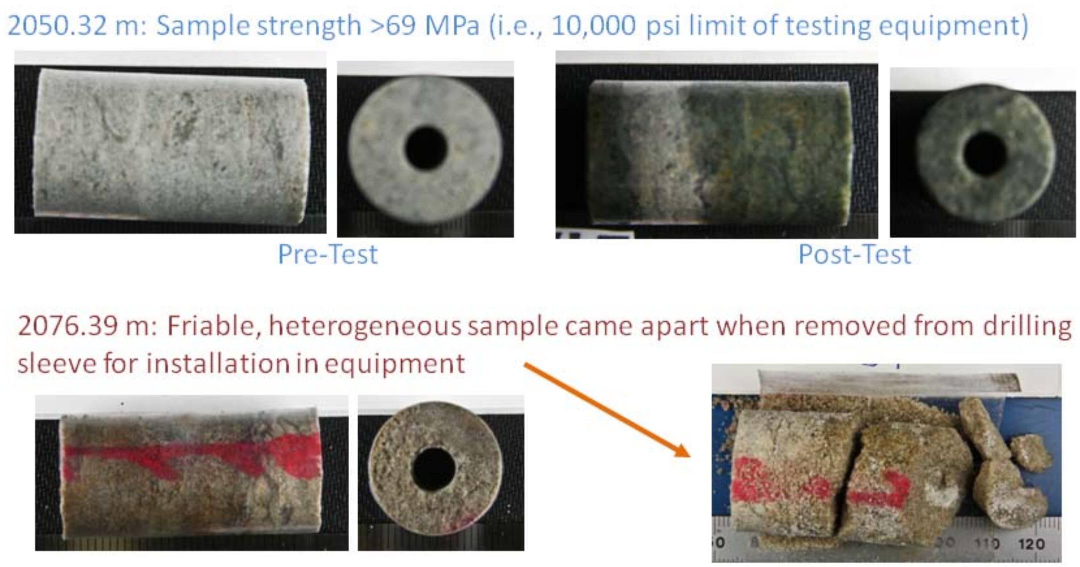

Figure 2-5. Summary of thick wall cylinder collapse test results.

3. BCS COMPRESSILITY MEASUREMENTS

Both uniaxial constant-lateral-strain and isotropic compressibility measurements were made on each BCS zone. Samples for tests were cleaned and their porosity measured during sample saturation at in-situ effective stress conditions. A 200,00 ppm NaCl brine was used for the pore fluid. Ultrasonic compressional and torsional shear velocities were also measured at selected stresses during these tests. The velocity data can be used to develop static-to-dynamic correlations for mechanical properties, which than can be used to estimate static properties outside of the measured zones

The uniaxial measurements are performed using a pore-pressure inflation-depletion protocol to measure deformations resulting directly from pore pressure changes, since the CO_2 injection process will be changing the pore pressure. The protocol is designed to cover the full range of possible pore pressures under the uniaxial-strain conditions, so mechanical properties will be measured over this range. The samples are taken to the estimated vertical and minimum horizontal stress[i] and pore pressure conditions of the reservoir, and then the pore pressure is increased to ~35 MPa, then decreased to ~1 MPa while holding the lateral dimension of the sample constant (typical to +/-1 micrometer or less). The uniaxial compaction coefficient, pore volume compressibility, depletion constant, under uniaxial strain conditions are obtained from these tests. The grain and bulk modulus and Biot coefficient at the reservoir stress conditions are also determined.

The isotropic compressibility test measurements above and below mean effective reservoir stress are done using a constant pore pressure protocol. Constant pore pressure was used to enable horizontal permeability measurements during the test. Samples were first compressed to the mean effective reservoir stress and equilibrated overnight (about 18 hours), sufficient time for sample and equipment to stabilize, and also provide a starting time for the uniaxial-strain loading. The grain and bulk modulus and Biot coefficient are measured at this point, then the sample is unloaded to near zero effective stress and reloaded to a maximum mean effective stress of 65 MPa, near the pressure limit of the equipment. Horizontal permeability measurements were made at 21.9 MPa, near the in-situ mean effective stress, and the maximum stress of 65 MPa, flowing through 6-mm diameter side taps across a diameter of the sample. The isotropic compressibility above and below the reservoir virgin stress conditions are reported below in section 3.2.

3.1. Uniaxial pore pressure inflation-depletion test results

Figure 3-1and Figure 3-2 show the measured uniaxial compaction coefficient and pore volume compressibility, respectively, for the three BCS zones. The plots show a relatively constant compressibility (C_m or C_p) for depletion and the first ~5 MPa of inflation, but an increasing compressibility above 25 MPa pore pressure. Constant compressibilities for pore pressures less than 25 MPa and the grain and bulk modulus and Biot coefficient measured at the in-situ conditions are summarized in Table 3-1.

[i] The minimum rather than the mean horizontal stress was used as a conservative choice that would maximize the range of pore pressure obtainable in the test.

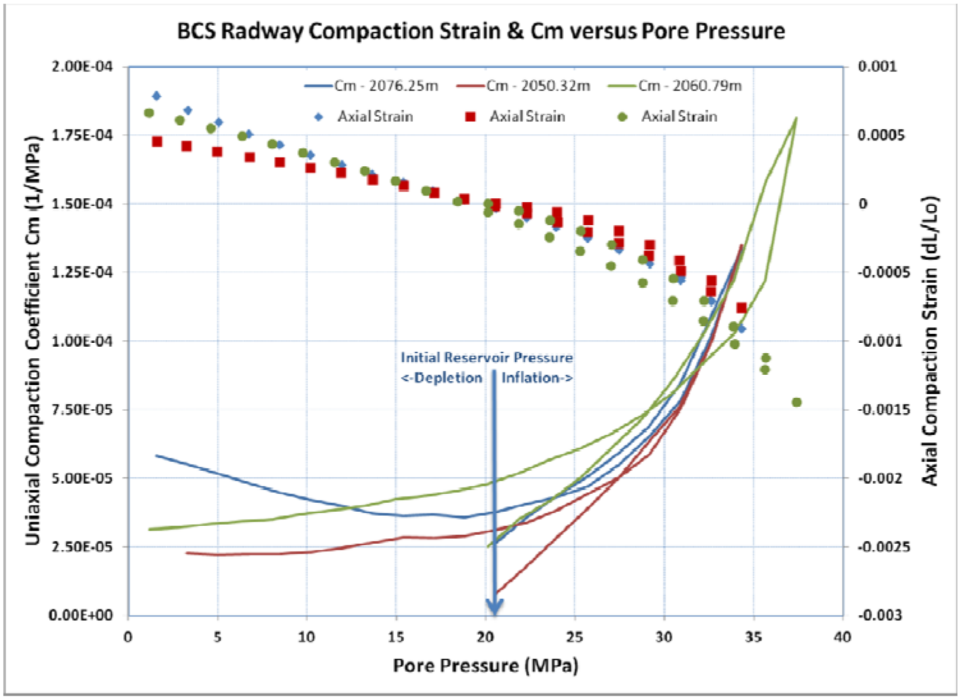

Figure 3-1. Uniaxial compaction strain and compressibility data plot.

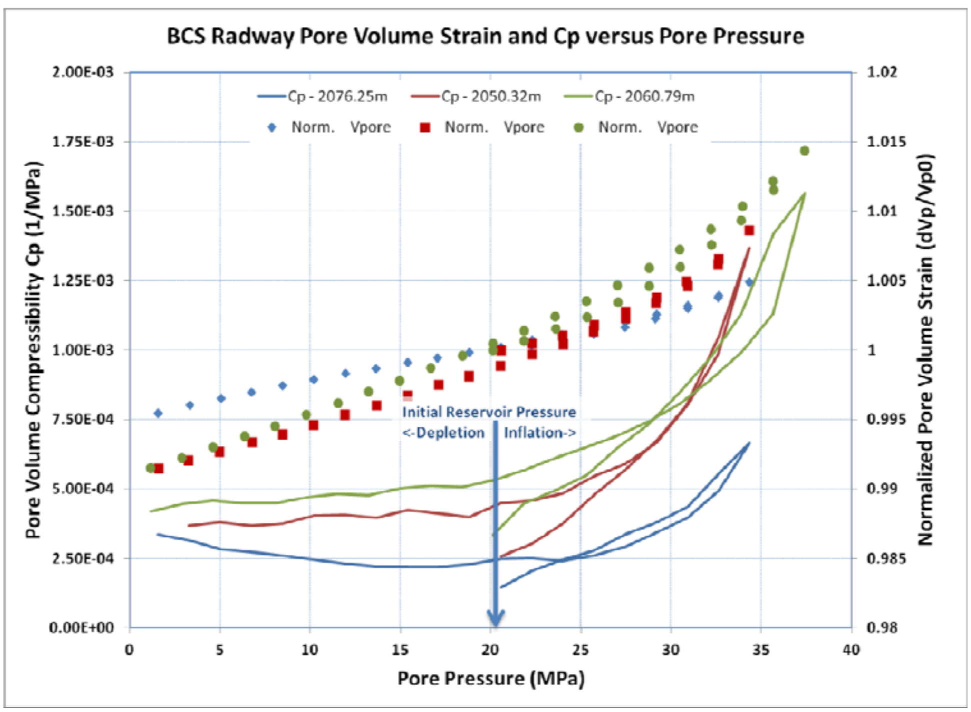

Figure 3-2. Pore volume strain and compressibility data plot.

Table 3-1. Constant uniaxial compressibility summary.

Sample Name	Set	Sample Depth (m)	Grain Modulus Kg (GPa)	Bulk Modulus Kb (GPa)	Biot Coefficient (1 - Kb/Kg)	Constant Uniaxial Compaction Coef. Cm (1/MPa)	Constant Pore Volume Compressibility Cp (1/MPa)	Constant Depletion Coefficient Gamma
RAD006A	1	2076.25	34.32	7.40	0.78	4.12E-05	2.44E-04	0.77
RAD055	2	2050.32	29.95	10.99	0.63	2.68E-05	4.06E-04	0.66
RAD074	3	2060.79	29.67	9.71	0.67	4.10E-05	4.91E-04	0.65

We believe the significantly increasing compressibility seen in Figure 3-2 at pore pressures above 25 MPa (i.e., effective stresses significantly below initial reservoir conditions) may be related to sample disturbance and may not reflect the in-situ reservoir behaviour. This is based on an examination of unstressed thin sections, which show some disturbed grain contacts. Figure 3-3 is an example unstressed thin section from virgin core material from 2050.10 m, where undisturbed contacts are marked with black arrows and red arrows mark channel-like pores between the grains that appear to be simply separated contacts. Such separated contacts have typically only been observed in thin sections from samples known to be disturbed. For this reason we recommend that as a base-case for reservoir and geomechanical modeling the compressibility properties be assumed constant with pore pressure equal to the values given in Table 3-1. To cover the possibility that these are not coring related features, but are actually present in the subsurface, an additional non-linear compressibility case can be done using the C_m and C_p values measured at 2060.79 m during the depletion from 37 MPa pore pressure. These values can be found in the Excel uniaxial data summary file BCSuniax.xlsx in the accompanying data DVD.

Ultrasonic velocity measurements were also made during the uniaxial-strain tests and are summarized in Figure 3-4. Similar to the static compressibility data, the velocities are relatively constant above the initial in-situ stress conditions, and show a marked decrease at pore pressures greater than 25 MPa, i.e., mean effective stresses 3 MPa or more below the estimated virgin in-situ value of 21.3 MPa. As expected, dynamic compressibilities calculated from the velocities are 60-70 percent of the static values.

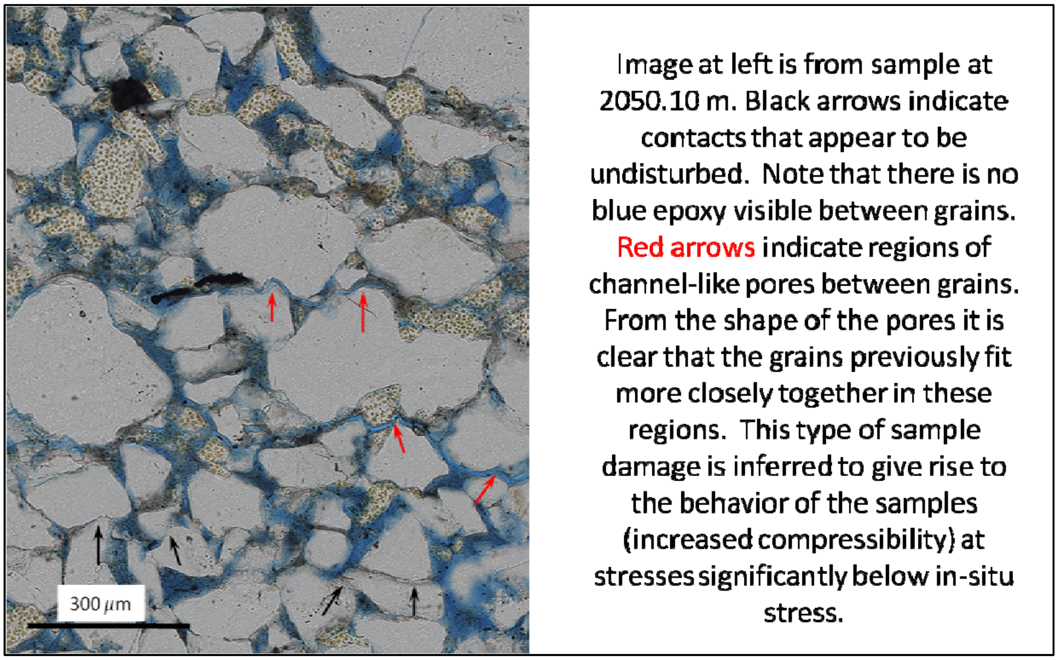

Figure 3-3. Unstressed thin section from untested material from 2050.10 m, showing intact and separated grain contacts.

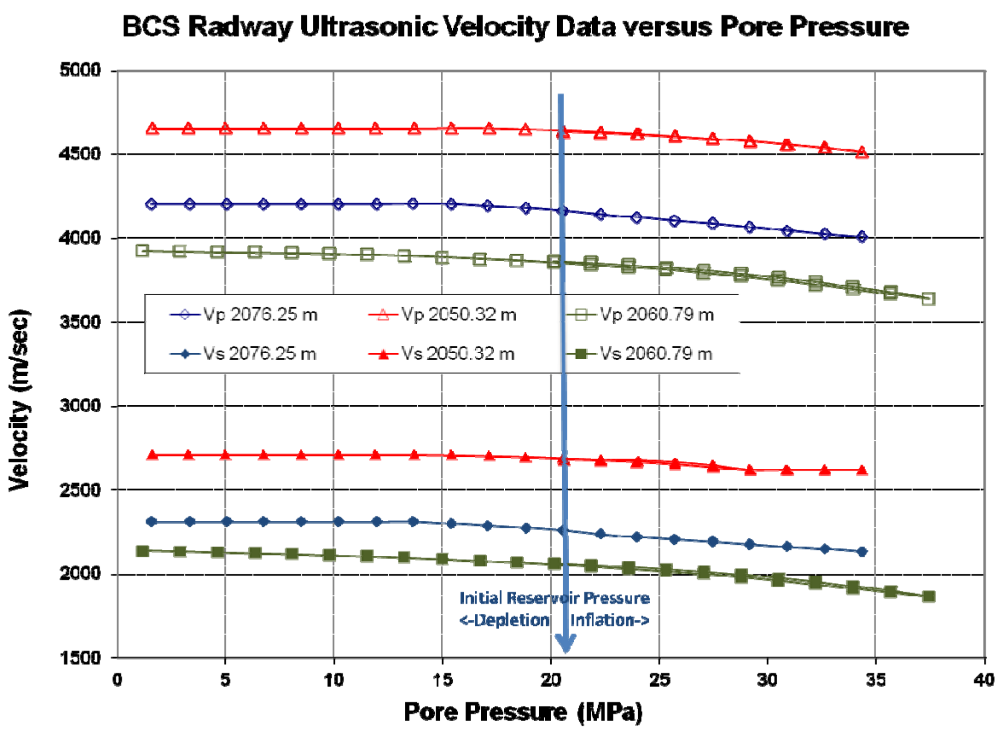

Figure 3-4. BCS uniaxial-strain test ultrasonic velocity data versus pore pressure.

3.2. Isotropic bulk compressibility test results

The isotropic compressibility test results are shown in Figure 3-5. As with the uniaxial-strain measurements, the bulk compressibility C_b is large near zero mean effective stress and reduces to an approximately constant value near and above the reservoir initial mean effective stress. For base case considerations a constant bulk compressibility has also been calculated using a linear fit to the bulk volume-mean effective stress data above 19 MPa. These constant C_b values and the measured initial in-situ stress grain, bulk modulus, Biot coefficient, porosity and permeability are summarized in Table 3-2. The detailed isotropic compression test data are provided in Excel file BCSisotropic.xlsx in the accompanying data DVD. Note that these files also report an isotropic pore volume compressibility for these tests. These are not explicitly reported here as these values are not appropriate for use in reservoir simulation since the bulk reservoir will not follow an isotropic stress path.

Ultrasonic velocities measured during the isotropic compression tests at a few points above initial reservoir mean effective stress are shown in Figure 3-6. These are roughly similar to those measured under uniaxial-strain conditions presented above in Figure 3-4.

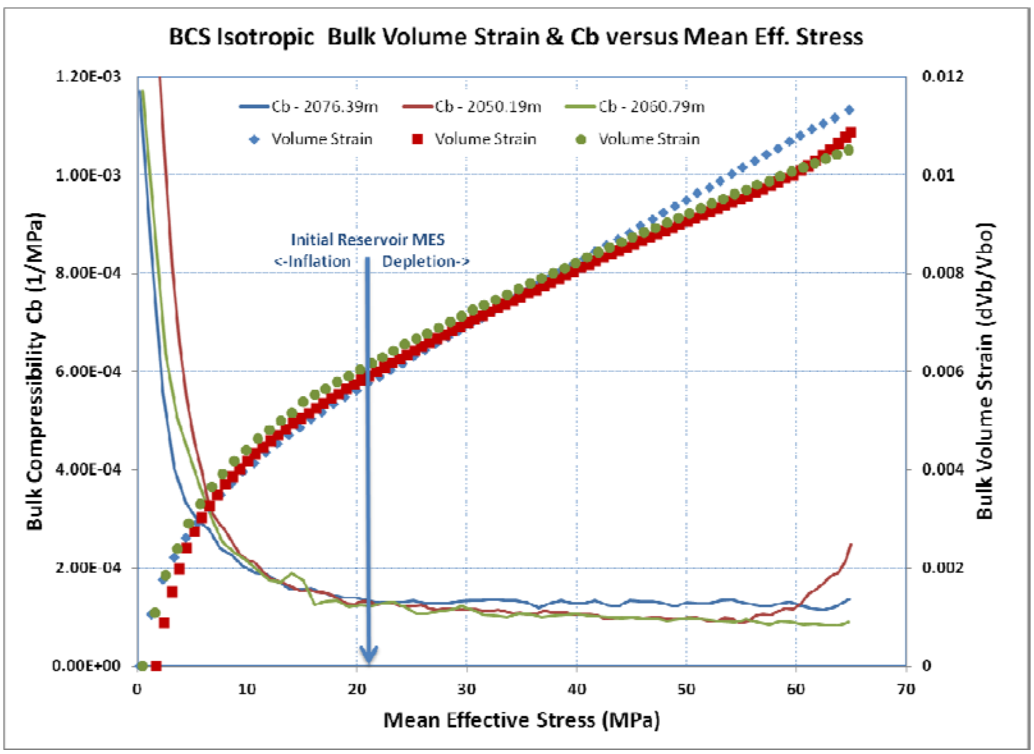

Figure 3-5. BCS isotropic compressibility and bulk volume strain data versus mean effective stress (MES). Estimated initial reservoir MES of 21.33 MPa indicated with blue arrow.

Table 3-2. Constant isotropic compressibility summary.

Sample Name	Set	Sample Depth (m)	Grain Modulus Kg (GPa)	Bulk Modulus Kb (GPa)	Biot Coefficient (1 - Kb/Kg)	Constant Bulk Volume Compressibility Cb (1/MPa)	Initial In-situ Porosity (%)	Permeability at In-situ Stress (mD)
RAD033	1	2076.39	21.86	8.57	0.61	1.29E-04	12.86	62
RAD043	2	2050.19	22.76	7.56	0.67	1.07E-04	8.22	<1.0*
RAD072	3	2060.79	21.89	7.74	0.65	1.01E-04	18.76	73

** This value is unrepresentative of the porous BCS. CT scan shows this sample to be very heterogeneous, with some tight horizontal layers and vertical streaks. Likely the side taps were placed within or across one of these tight streaks, resulting in the very low permeability measurement.*

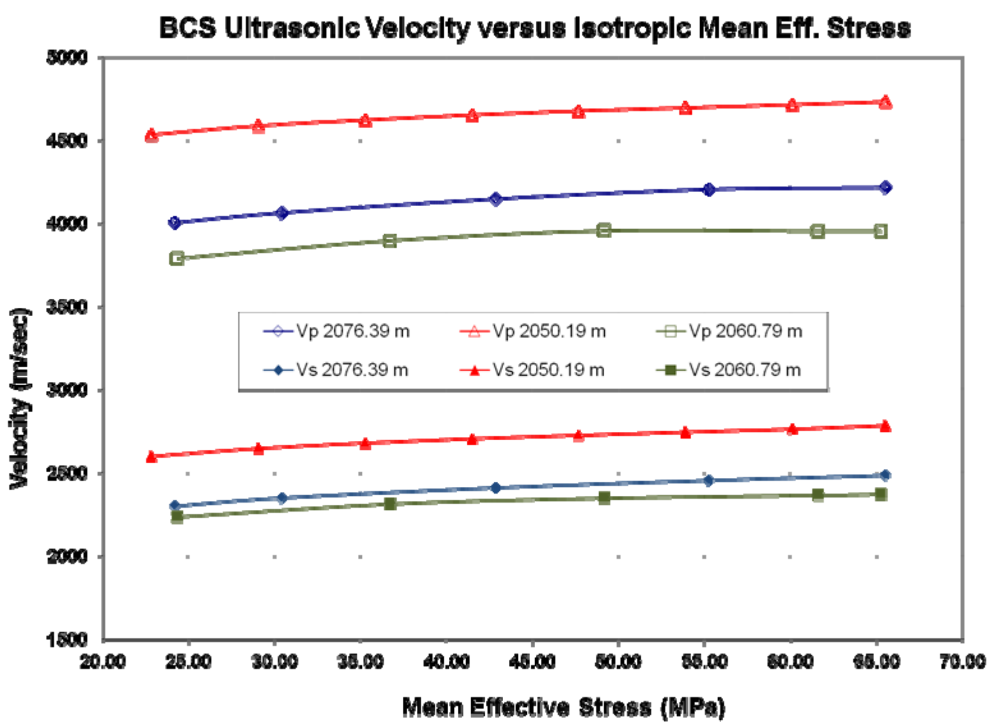

Figure 3-6. BCS isotropic compression test ultrasonic velocity data versus mean effective stress.

4. THERMAL EXPANSION MEASUREMENTS

Thermal expansion measurements were planned to be done using equipment under development in the Shell High Temperature Geomechanics Laboratory. Delays in this development led to three samples being sent to TerraTek, Inc., Salt Lake City, Utah, for thermal expansion measurements. However, TerraTek had unexpected delays as well, and at the time of publication of this report expects to deliver these measurements end January, 2012. Meanwhile, our equipment has been completed, so two additional thermal expansion measurements have been made on available Radway core material. One sample is RAD051, the TWC sample that did not fail. The second sample is RAD091. This sample is taken from directly below the zone 3 samples, but appears to have much higher shale content and is substantially denser than any of the other plugs tested. It is more likely representative of some of the non-reservoir quality rock within the BCS.

The thermal expansion coefficient has been measured between 35C and 100C. Samples were installed into the thermal expansion apparatus, brought to a nominal 1MPa confining pressure, and then the temperature was increased in steps and held constant for 10 hours at each temperature to allow equilibration. The stabilized axial strains at the end of each hold period are used to calculate the linear thermal expansion coefficient. Hold temperature values of 35C, 50C, 75C, and 100C are used for these tests. Results are summarized in Table 4-1.

Table 4-1. Linear Thermal Expansion Summary

Sample Name	Set	Sample Depth (m)	Linear Thermal Expansion Coefficient (x10^-6/C)	Temperature Range (C)
RAD051	2	2050.32	10.7	35-100
RAD091		2060.89	9.9	35-100

5. SUMMARY DISCUSSION

The report documents a series of geomechanical tests on BCS core from three zones in the Shell Canada Radway well SCL 08-19-59-20W4. Suites of triaxial compression strength tests provide loading Young's modulus (YM), Poisson's ratio, friction angle and cohesion measurements. Uniaxial constant-lateral-strain pore pressure depletion tests provide uniaxial compaction coefficient C_m and pore volume compressibility C_p measurements appropriate for estimating compaction/subsidence and reservoir pore volume change behaviours. Isotropic bulk volume compressibility C_b tests provide bulk and pore volume change behaviour under isotropic compression stress path. The uniaxial strain and isotropic compression tests also provide estimates of the formation Biot coefficient. Although the compressibility measurements show a marked non-linear increase as the rocks approach zero effective stress, unstressed thin section analysis indicates this behaviour may be related to sample disturbance. For base case modeling considerations we recommend using constant compressibility values estimated from the test data ranging from 3 MPa below initial in-situ effective stress conditions to the maximum effective stress achieved in the test (i.e., pore pressures below 25 MPa for the uniaxial-strain tests).

The thermal expansion measurement on sample RAD051 is currently the only measured value on rock comparable to the other measurements. That value is 1.07×10^{-5}/C. This report will be updated with the additional measurements after they become available.

The compressive strength data are similar enough that the following average values are recommended : Friction angle – 39+/-3 degrees ; Cohesion – 11.3 +/- 1.6 MPa.

There are insufficient TWC data to provide any quantitative conclusions. Further testing would be required to provide TWC strength data suitable for developing log correlations for sanding predictions.

The different measurements under different stress paths provide a range of mechanical parameters for the BCS formation. The various constant compressibility or modulus values (YM, C_m, C_p, C_b) around initial in-situ stress conditions have standard deviations of roughly 30% across the samples measured. Using measured parameters from one test type to predict other linear poro-elastic parameters does not always gives values within these standard deviations (e.g., C_m calculated from the triaxial compression measured YM and Poisson's ratio). In particular, the measured depletion constant and Biot coefficient from the uniaxial compaction tests implies a Poisson's ratio near zero, compared to the triaxial measured range of 0.15-0.36. This gives an indication of the limits of treating the material as a perfect linear poro-elastic material.

The authors do not have information on how representative the three tested zones are to the BCS formation as a whole. None the less, considering only the measurement suite reported here, a self-consistent set of linear poro-elastic parameters are presented in Table 5-1. These are based on the average of the Cm, Cp and depletion constant values measured in the uniaxial-strain tests (the closest stress path to likely field operations), and adjusts the Biot coefficient/grain modulus to yield a finite Poisson's ratio a little below the lower end of the range measured in the triaxial compression tests. Clearly any reservoir or geomechanical simulations or calculations done using these values should also include significant parameter sensitivity calculations to honour at least the full range of behaviour seen in these tests.

Table 5-1. Consistent BCS rock geomechanical parameter set (red values calculated from black values):

Symbol	Value	Units	Measured Range Across Tests	Parameter Description
Cmp	0.036	1/GPa	0.027 - 0.041	Uniaxial compaction coefficient under depletion
Cpp	0.38	1/GPa	0.24 - 0.49	Uniaxial pore volume compressibility under depletion
γ	0.69	--	0.65 - 0.77	Horizontal depletion constant
α_B	0.80	--	0.63 - 0.78	Biot coefficient
ν	0.12	--	0.15 - 0.36	Poisson's ratio from α, γ
E	21.33	GPa	15.1 - 29.5	Young's Modulus from Cmp, ν, γ
G	9.54	GPa	6.3 - 10.8	Shear modulus from E, ν
K(elas)	9.30	GPa	7.3 - 36.2	Drained bulk modulus from E, ν
Ks	46.48	GPa	21.9 - 34.3	Grain modulus from α, K
θ	41.3	fractional	37.2 - 44.4	Friction Angle
c	10.3	MPa	9.4 - 12.5	Apparent cohesion
α_T	1.03E-05	1/C	0.99e-5 - 1.07e-5	Linear thermal expansion coefficient

REFERENCES

El Mahdy, R., H. de Groot, A. Simone (2011) Seal Integrity and Fracture Pressures, Quest CCS Project Document Number 07-3-ZG-7180-0012

APPENDIX 1. DETAILED PETROLOGY OF THE BCS ZONES TESTED

A suite of 6 Computer-Assisted Petrology (CAP) analyses was performed on the uniaxial-strain and 21.3 MPa confining stress (i.e., in-situ mean effective stress) triaxial test samples. The analyses were performed on post-test thin sections. In the case of the uniax samples, the sands were so incompressible that there was very little or no sample damage to interfere with the image analysis. In the case of the triax samples, the damage zones associated with shear failure are so narrow that undisturbed portions of the sample were readily available for analysis. In addition to the CAP analysis, Scanning Electron Microscope (SEM) backscattered imaging and X-ray dot mapping were performed in order to assess the origin and mineralogy of dispersed clay in the pore system of some samples, and to clarify the mineralogy of feldspar overgrowth cements.

A1.1 Zone A (Set1): 2076 m

The sand at 2076 meters is the coarsest grained (averaging 1.6-1.8 phi, or upper medium sand) and most quartzose (framework more than 95% quartz) of the units examined. The feldspar grains present are predominantly observed in finer-grained laminations. The zone exhibits variable porosity ranging from 12.3 to18.8%, based on the two measured values of the isostatic (RAD072) and uniax (RAD074) plugs, respectively. Both samples analyzed in thin section are from the higher porosity end member of this unit, with average porosities between 21.4-21.7%. Quartz overgrowth and feldspar overgrowth (albite) cements are present in volumes less than 1% of the whole rock. Other cements observed in this interval include nodular analcime (a sodium zeolite; I. Espejo, pers. comm.), and rare TiO_2 (sphene/anatase) and potassium-feldspar (K-feldspar) cements (see accompanying images below). Intergranular volumes observed in this unit range from 20-24%, indicating that compaction has dominated porosity loss in this unit relative to cementation. This observation is true for all three of the units examined in this study. The in situ triax sample did not fail in a discrete shear zone that penetrated the entire sample, but rather exhibits localized failure in a coarse grained/higher porosity lamination. This is consistent with this sample failing at significantly lower deviatoric stress (117 MPa as opposed to 134 MPa) than the other two samples tested at the same 21.3 MPa confining stress.

Radway 002 2076.25 m, Post-test Triax at In-Situ Stress

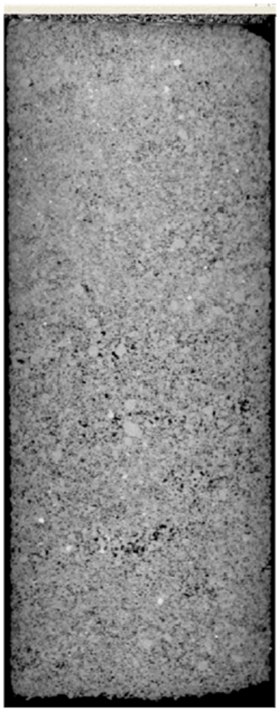

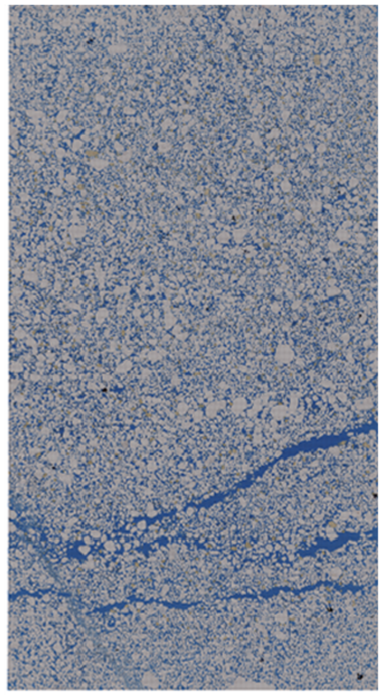

Gray scale image of CT scan of plug 002 (far left) and transmitted light scan of post-test companion thin section (middle). Note that failure surface does not penetrate the entire sample but is restricted to a zone of higher porosity (22% in undisturbed portion of failed zone, compared to 17% in the intact zone). Image A shows higher magnification view of potassium feldspar grains (stained yellow) with authigenic albite overgrowths (black arrows). Image B at lower left shows authigenic TiO_2 minerals (sphene/anatase; red arrows). Image C shows pore filling dispersed clay matrix, (green arrows) both of which occur locally through the sample.

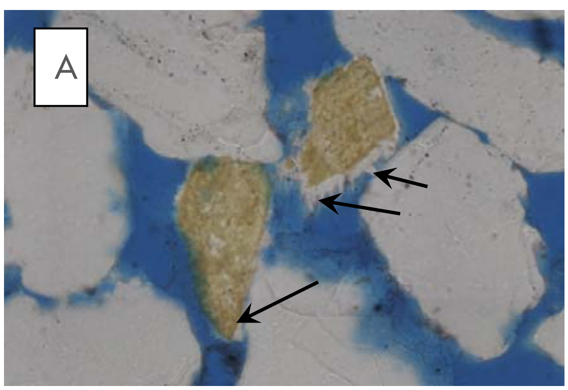

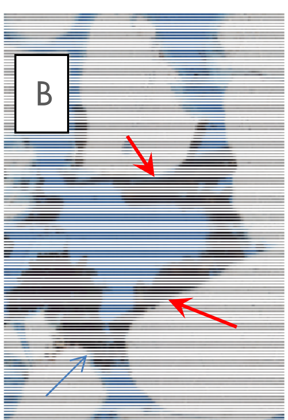

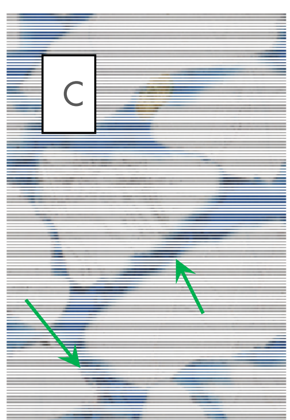

Radway 002 2076.25 m

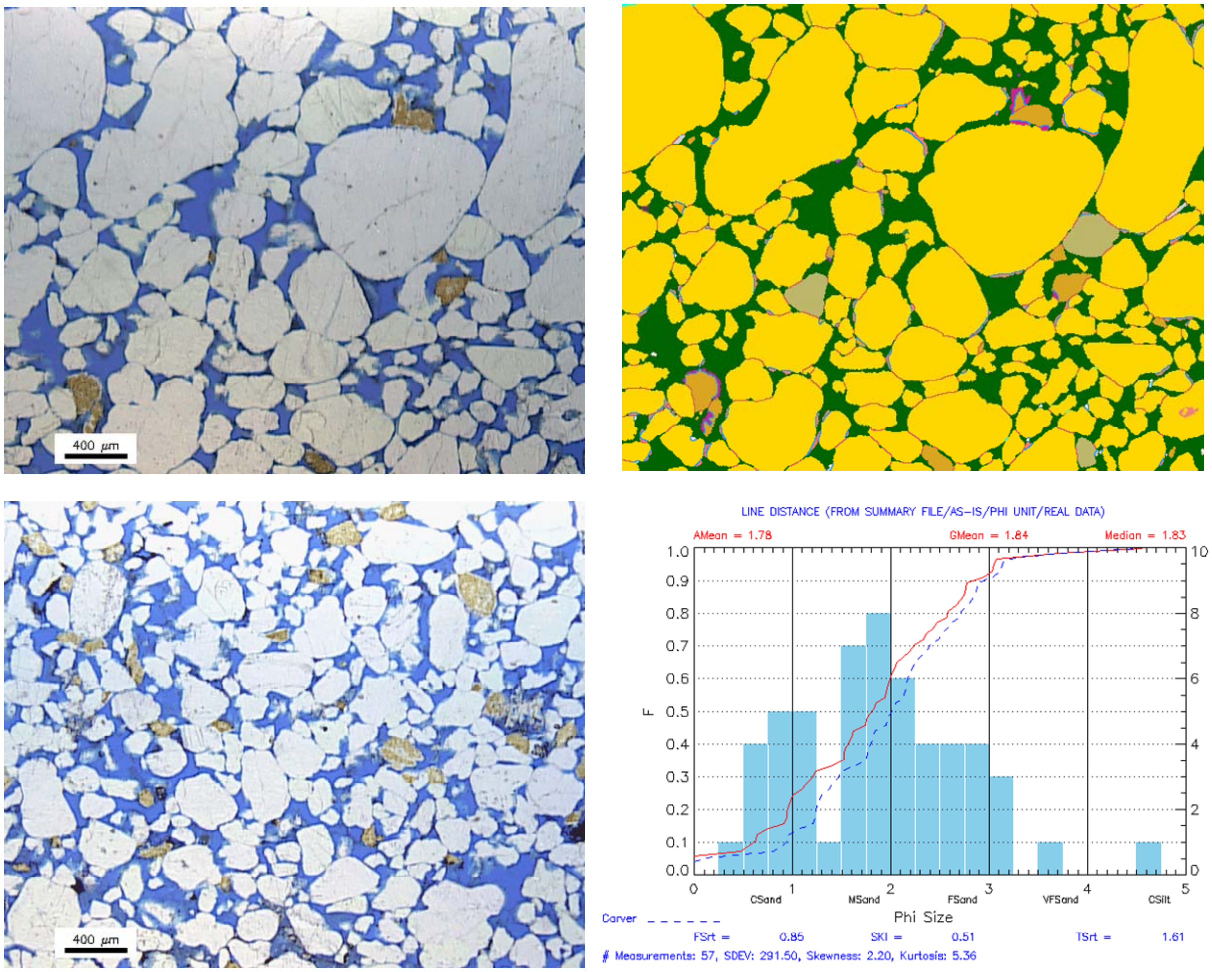

Transmitted light images of plug RAD002 and companion CAP analysis where completed. Note the highly variable texture present on a thin section scale. Potassium feldspar grains are typically finer grained than associated quartz grains, and potassium feldspar is present in higher volumes in finer grained laminae (lower right). Mean grain size is 1.75 phi (upper medium sand) and Trask sorting is 1.6 moderately poor. Thin section porosity is 20.4%.

Radway 002 2076.25 m

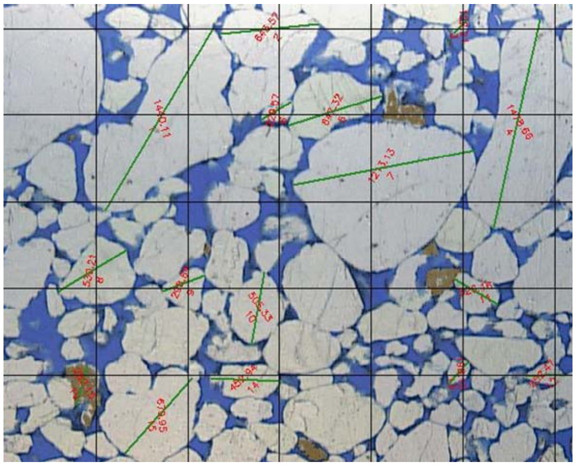

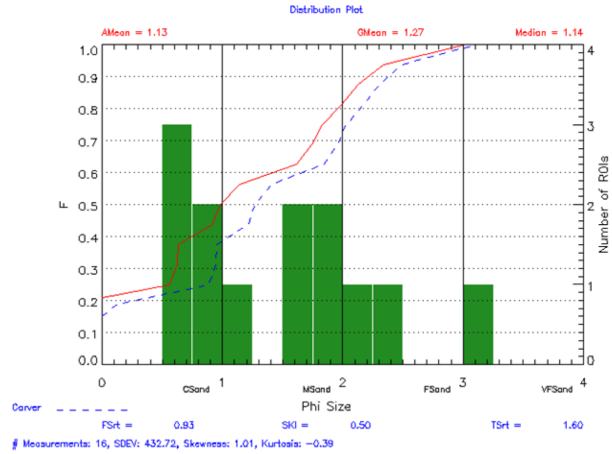

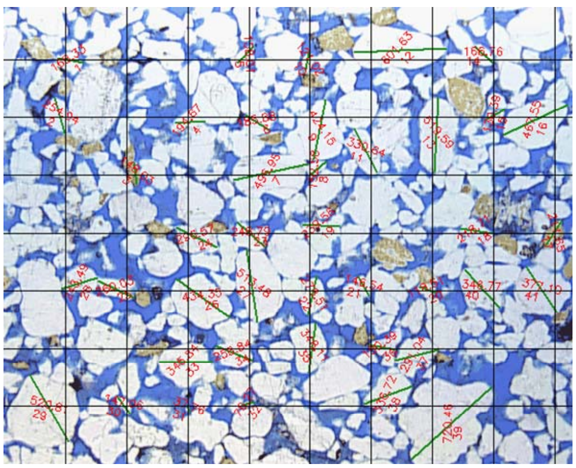

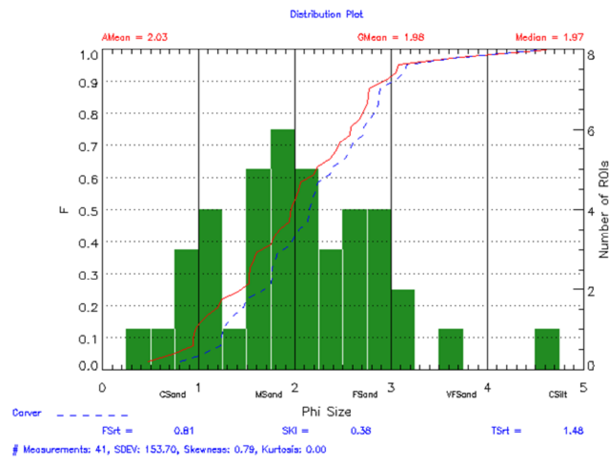

Grain size analysis for the two analyzed images. A grid is superposed on the image such that, to the greatest extent possible, the grid size approximates the size of the largest grain in the field of view. Apparent long axis is then measured at grid points that intersect framework grains. Size distributions for each image are shown; the summary size distribution plot is shown in the previous figure.

Radway 002 2076.25 m

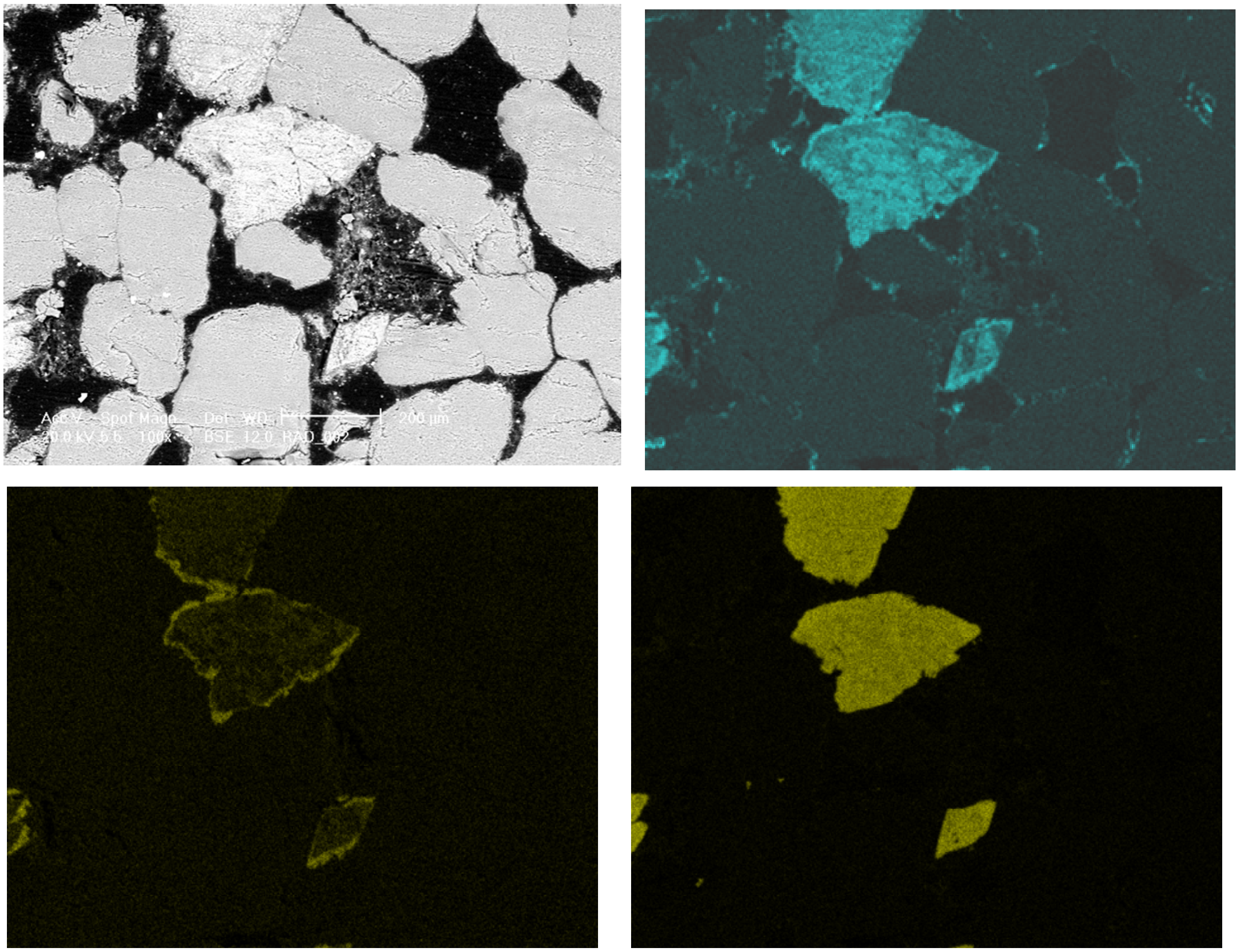

Backscattered electron image of plug RAD002 and major element X-ray dot maps of the same field of view. Map above right shows the distribution of aluminum, and map at lower right shows the distribution of potassium associated with K-feldspar grains in this field of view. Map at lower left shows the distribution of sodium. Note that the authigenic rims on the K-spar grains are albite (sodium feldspar, or Na-feldspar).

Radway 002 2076.25 m

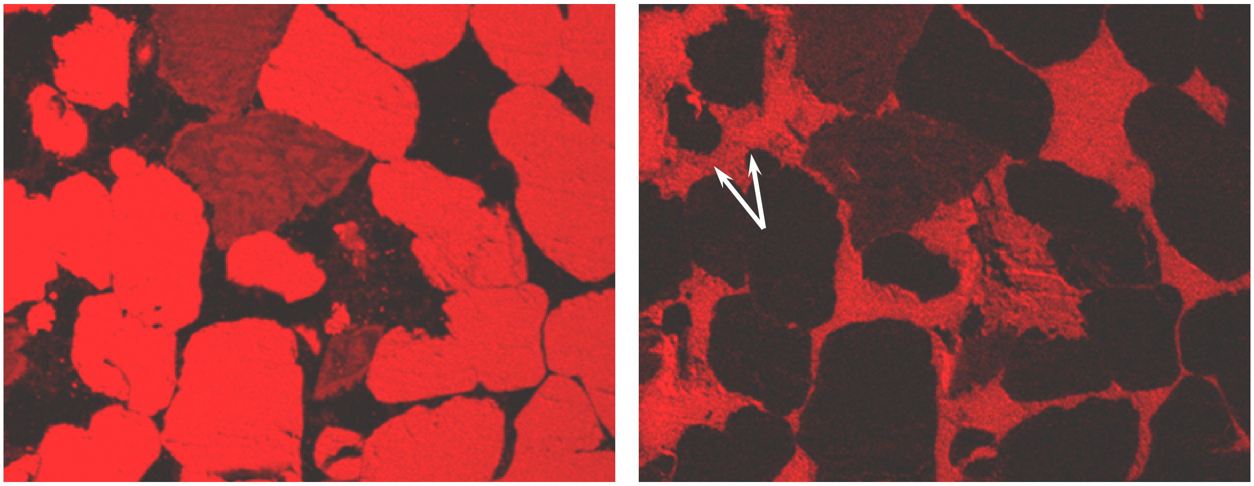

X-ray dot maps showing the distribution of silicon (above left) and carbon (above right). Silicon is present in quartz framework grains and overgrowth cements (bright red) and to a lesser extent in feldspar grains (dull red). The carbon response is associated with the epoxy that the sample is impregnated with and thus gives an indication of porosity distribution. Where response is dim, micropores associated with dispersed clay in the sample are indicated (white arrows; compare with backscattered-SEM (BSEM) image to see the distribution of clay in the pore system).

Radway 002 2076.25 m

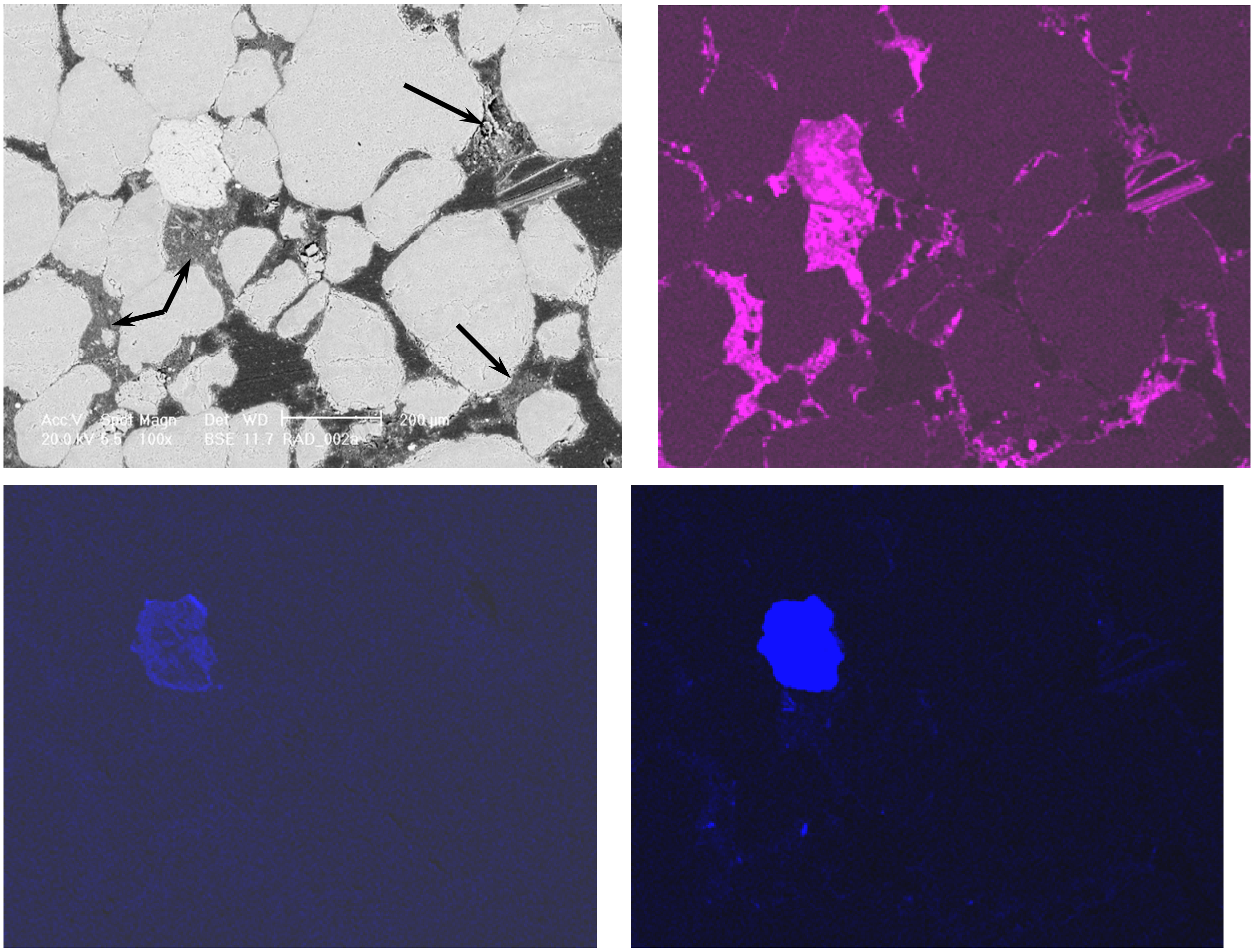

Backscattered electron image of plug RAD002 and major element X-ray dot maps of the same field of view. Map above right shows the distribution of aluminum, and map at lower right shows the distribution of potassium associated with K-feldspar grains in this field of view. Map at lower left shows the distribution of sodium. Note that significant aluminum is associated with pore filling clay indicated by black arrows in the BSEM image.

Radway 002 2076.25 m

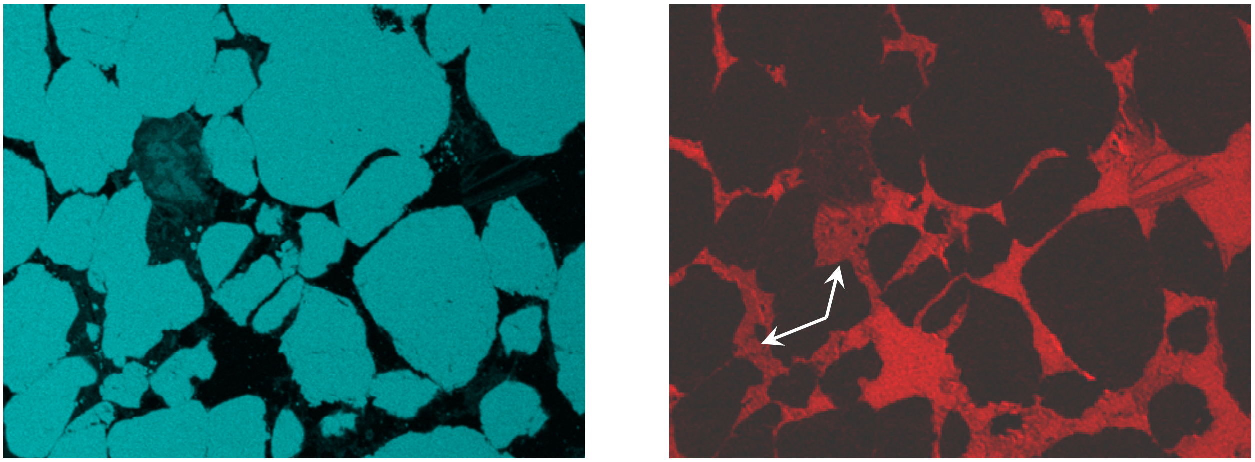

X-ray dot maps showing the distribution of silicon (above left) and carbon (above right). Silicon is present in quartz framework grains and overgrowth cements (bright blue) and to a lesser extent in feldspar grains (dull blue). The carbon response is associated with the epoxy that the sample is impregnated with and thus gives an indication of porosity distribution. Where response is dim, micropores associated with dispersed clay in the sample are indicated (white arrows; compare with BSEM image to see the distribution of clay in the pore system).

Radway 006a 2076.25 m

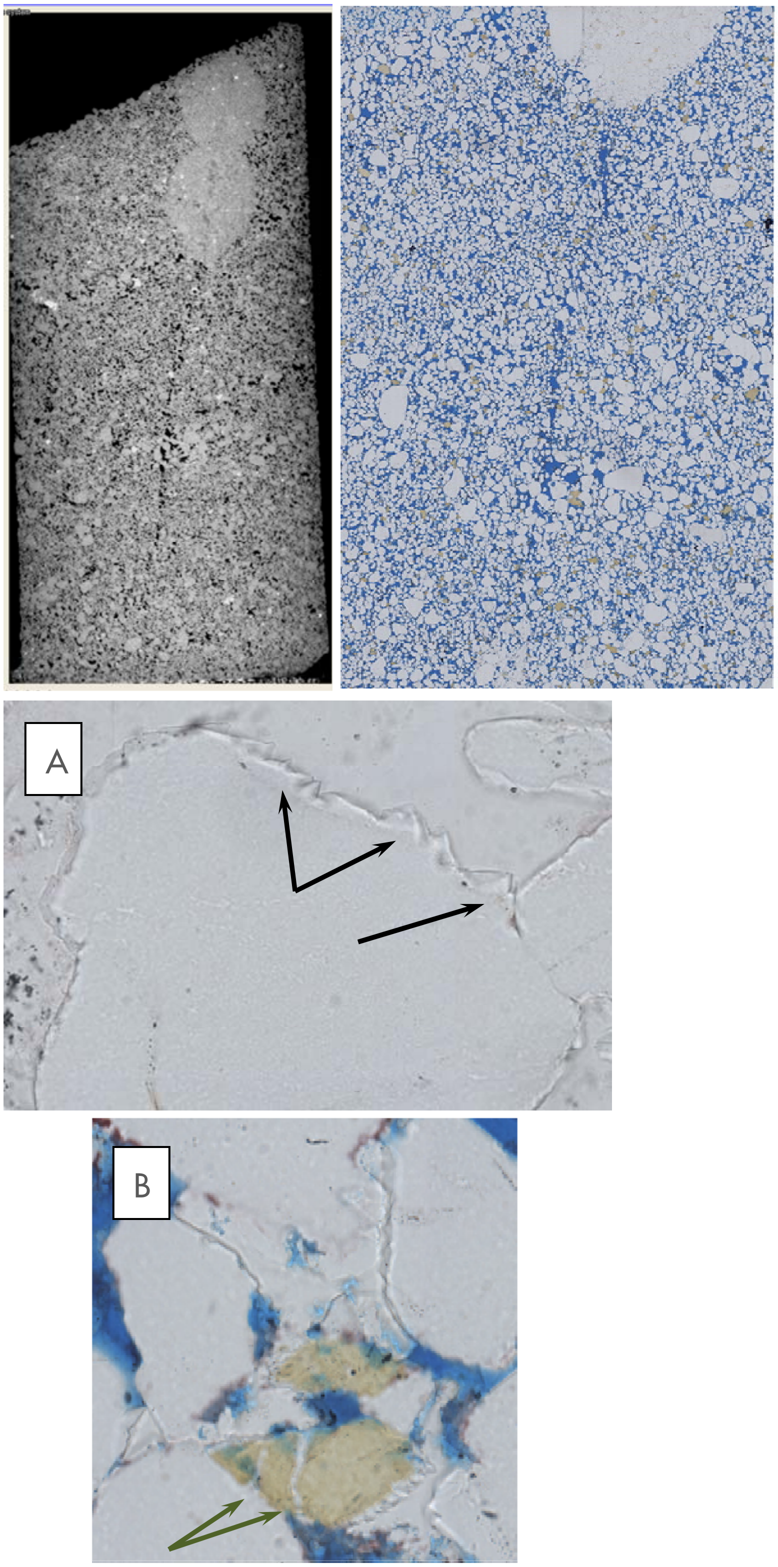

Gray scale image of CT scan of plug RAD006a (left) and transmitted light scan of companion thin section (middle). Image A shows higher magnification view of analcime nodule (black arrows indicate incipient quartz overgrowths that predate analcime precipitation). Image B shows an area where analcime cement is partially dissolved and is observed infilling a fracture in a potassium feldspar framework grain (green arrow).

Radway 006a 2076.25 m (Post-test Uniax)

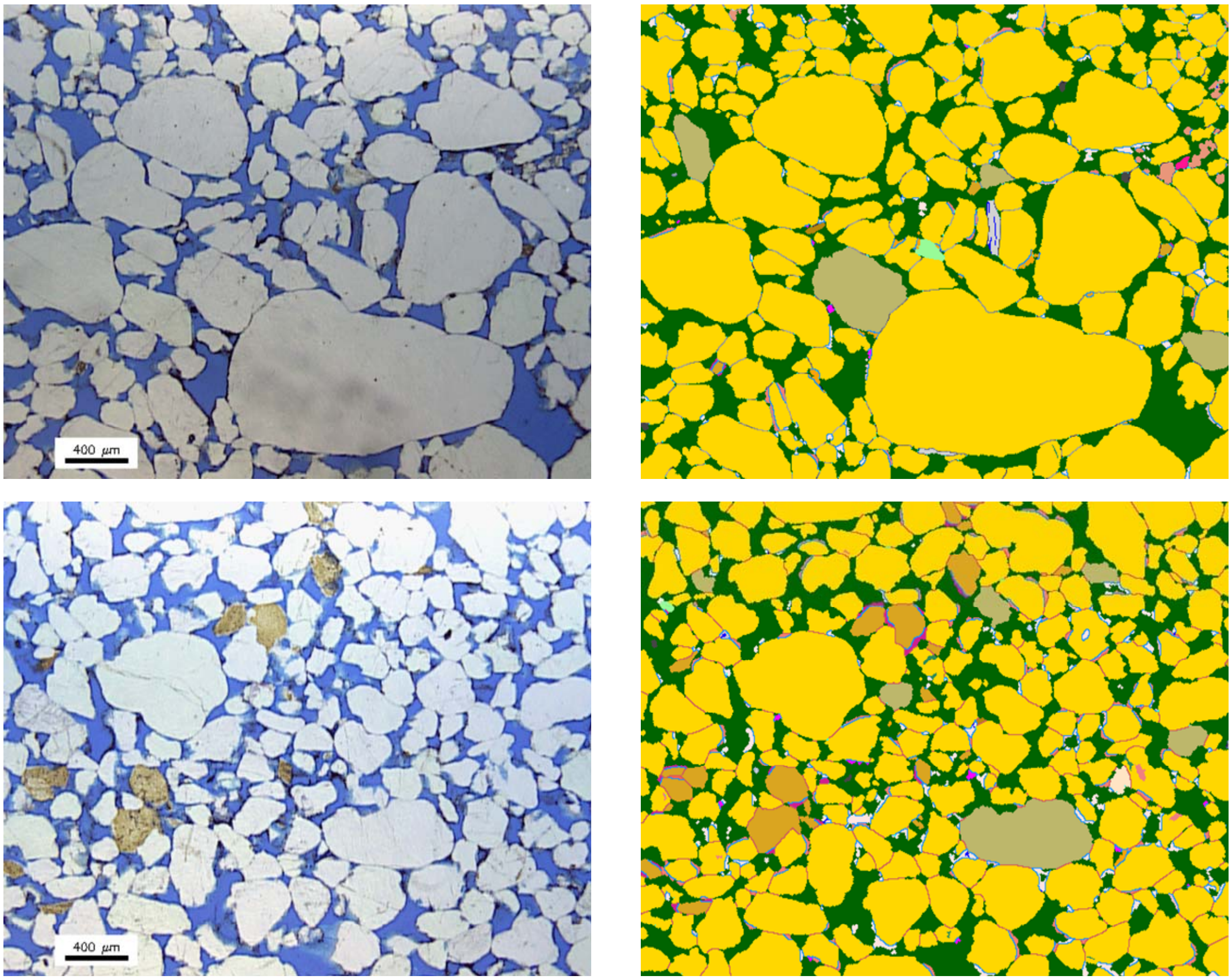

Transmitted light images of plug RAD006a and companion CAP analysis. Note the highly variable texture present on a thin section scale. Potassium feldspar grains are typically finer grained than associated quartz grains, and potassium feldspar is present in higher volumes in finer grained laminae (lower right). Thin section porosity is 21.7% (measured plug porosity is 21.3%).

Radway 006a 2076.25 m

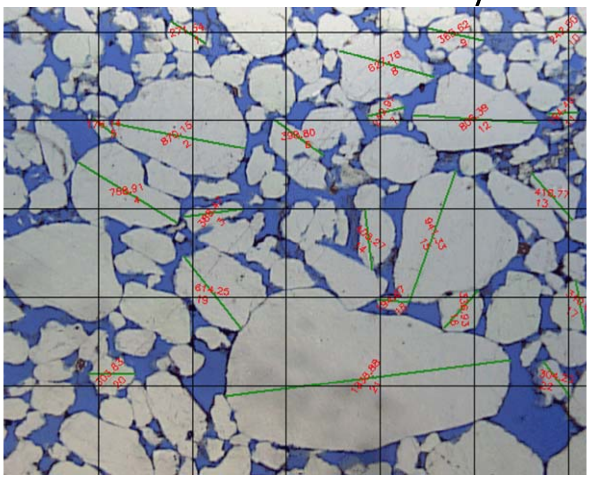

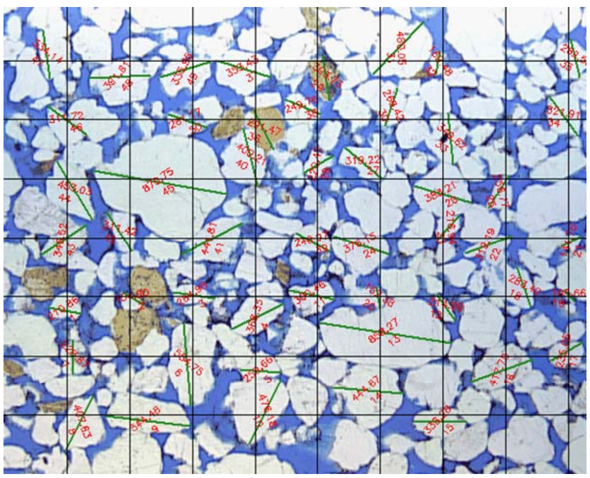

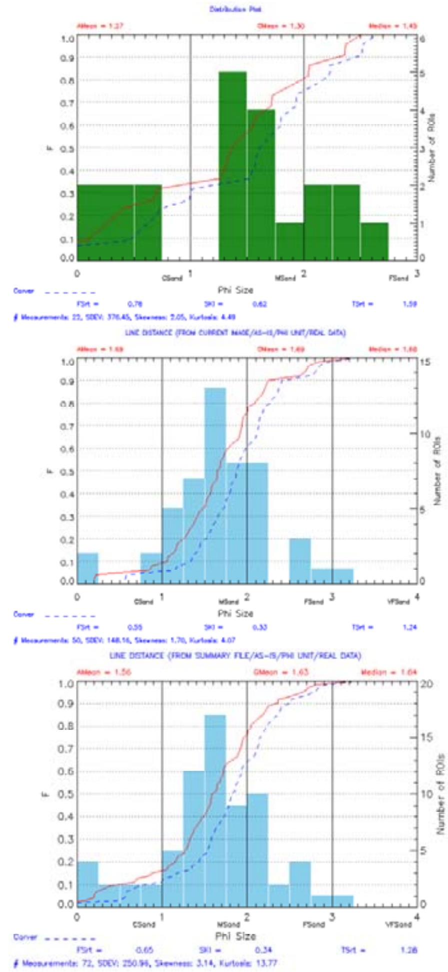

Grain size analysis for the two analyzed images. Size distributions for each image are shown; the summary size distribution plot is shown at the bottom. Mean size is 1.56 phi (upper medium sand) and Trask sorting is 1.4 (moderately sorted).

Radway 006a 2076.25 m

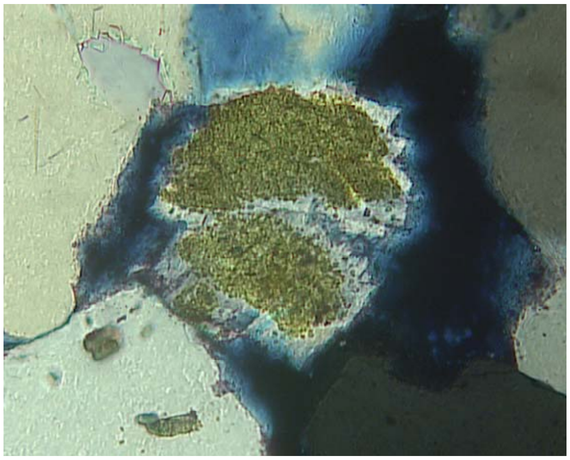

Light gray rims around potassium feldspar grains (stained yellow) are authigenic albite overgrowths (see Na dot map for sample 002).

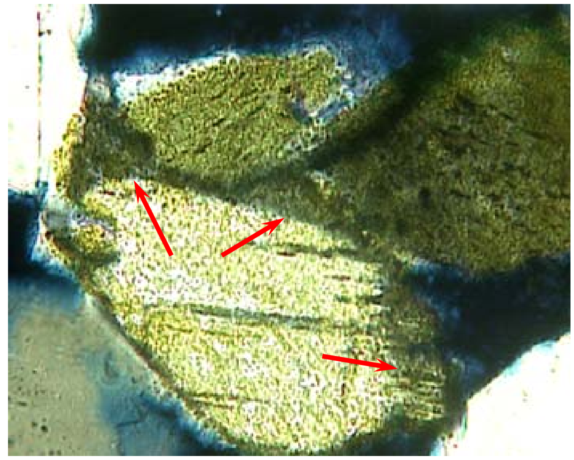

Dark rims around potassium feldspar grains (stained yellow; red arrows) are authigenic Kspar overgrowths (note that they appear to be in growth position binding adjacent detrital grains together).

A1.2 Zone B (Set 3): 2060.8 m

The sand at 2060.8 meters is the finest grained (averaging 3.2-3.25 phi, or upper very fine sand) and most feldspathic (framework on the order of 75% quartz) of the units examined, and is locally extremely rich in biotite mica (17% of total volume by segmentation). The feldspar grains present are predominantly K-feldspar. The zone exhibits highly variable texture , as suggested by microCT scanning of plugs and large format thin section observations. The presence/absence of bioturbation and micaceous lamina may result in variable flow and strength properties. Both CAP analyses are in clean (non-micaceous) portions of the samples. Average porosity in the thin sections examined ranges from 20.7-22.3%. Measured plug porosities range from 12.3-18.8%. This variability is most likely a function of the degree of bioturbation and mica content. Quartz and feldspar overgrowth cements each average on the order of 1.3% of the whole rock volume. The most common feldspar cement observed in this interval is K-feldspar overgrowths, although a trace of albite overgrowth cement is observed. Intergranular volumes observed in this unit range from 24-26%. Although the samples from this depth displayed a wide range in plug porosity this unit is the slowest unit acoustically regardless of the relative porosity as compared to the other samples in the data set. This is inferred to result from the high volume of potassium feldspar in the framework.

Radway 078 2060.79 m Post-Test Triax at In Situ Stress

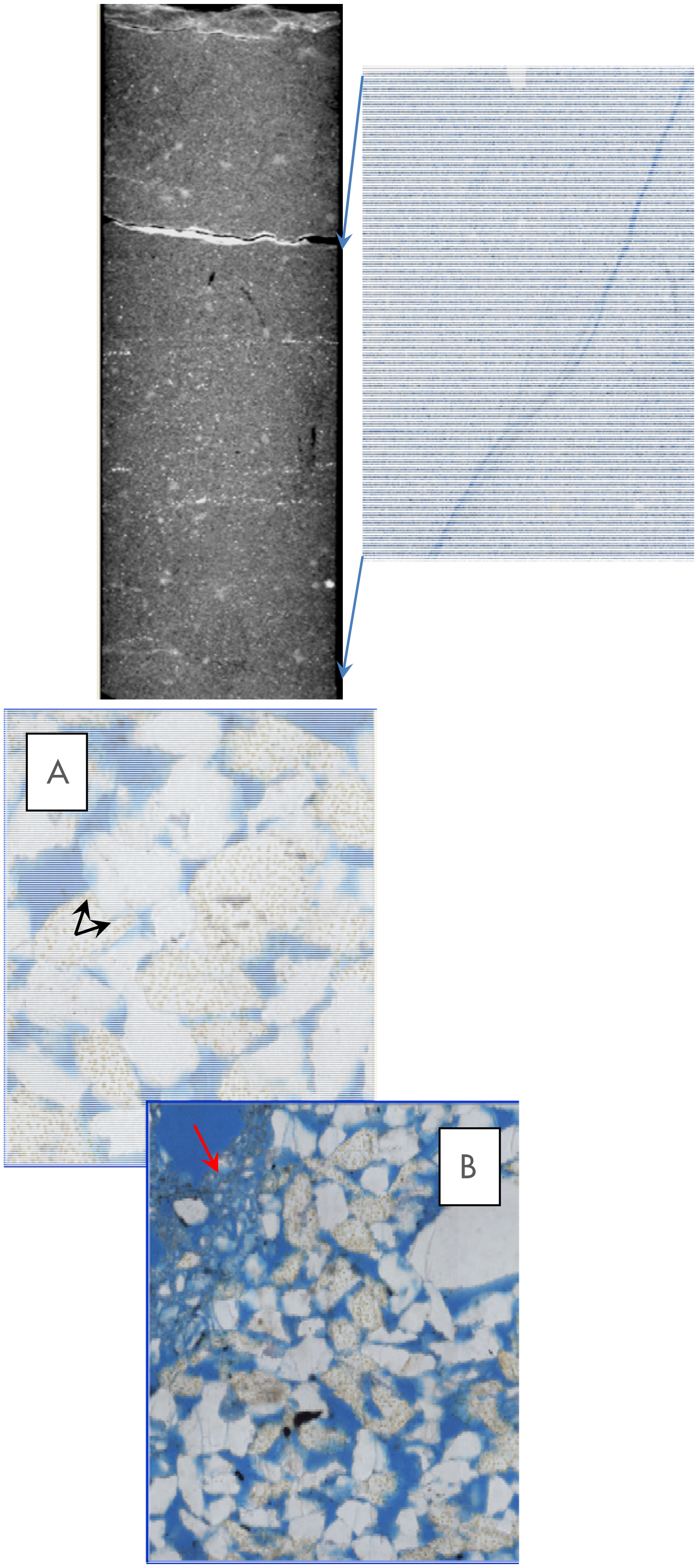

Gray scale image of CT scan of plug RAD078 (left) and transmitted light scan of companion thin section (middle). Note that this sample is much cleaner and more homogeneous than plug RAD072. Obtaining "twins" for a suite of measurements for this sample was not possible. This is further suggested by porosity measurements of RAD072 and RAD074, which varied from 18.8 to12.3 %, respectively. Image A shows that both quartz and feldspar overgrowth cements are common. In this sample both K-spar (black arrow) and albite overgrowths are present. Figure B illustrates that sample damage rapidly decreases away from zone of failure (red arrow).

Radway 078 2060.79 m

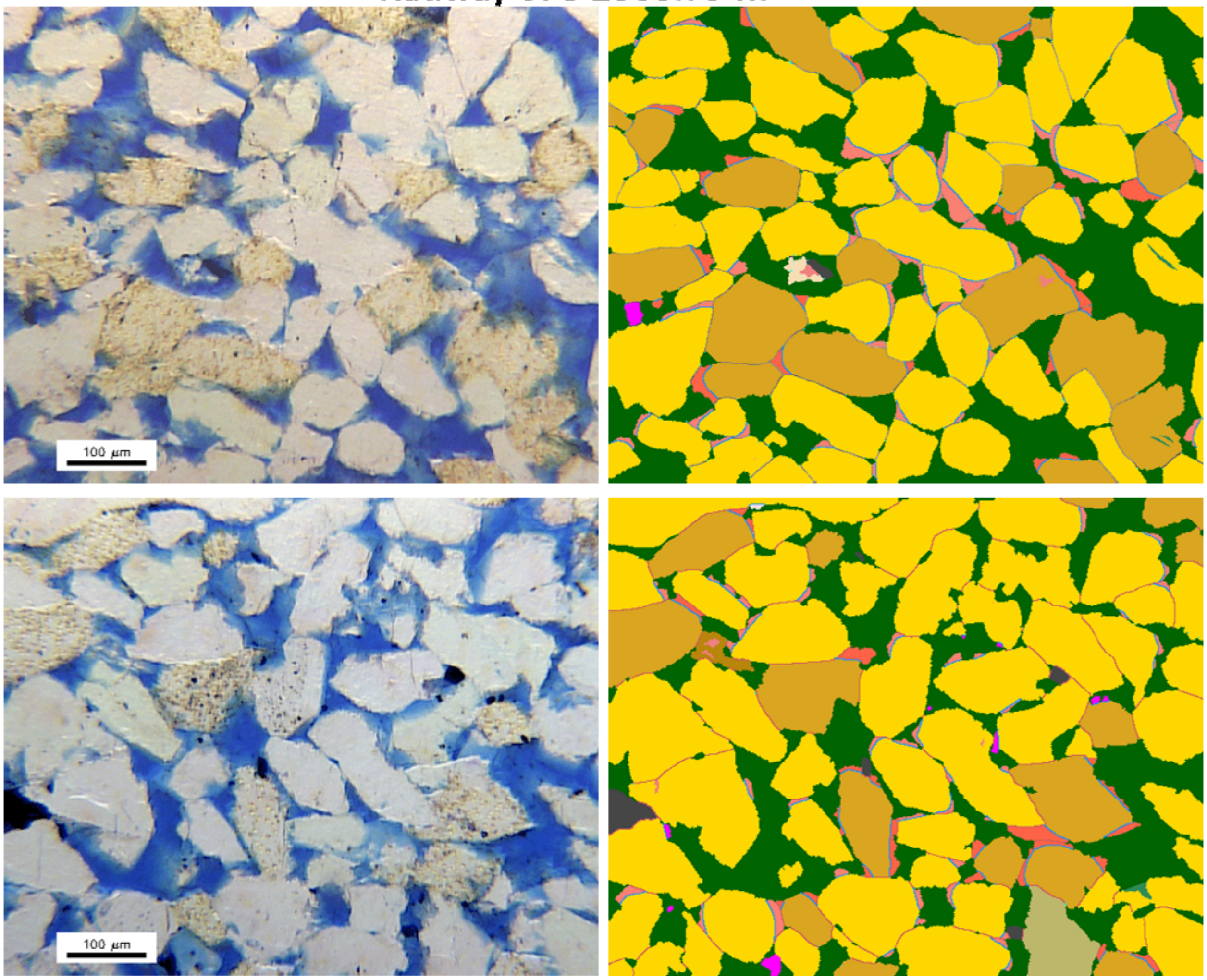

Transmitted light images of plug RAD078 and companion CAP analysis. Note that only the coarse grained component is represented in this analysis. Dolomite cement is present in the upper portion of both images and post dates quartz overgrowth precipitation, at least in part. Sutured contacts between quartz grains are common (red arrows). Thin section porosity is 22.3%.

Radway 078 2060.79 m

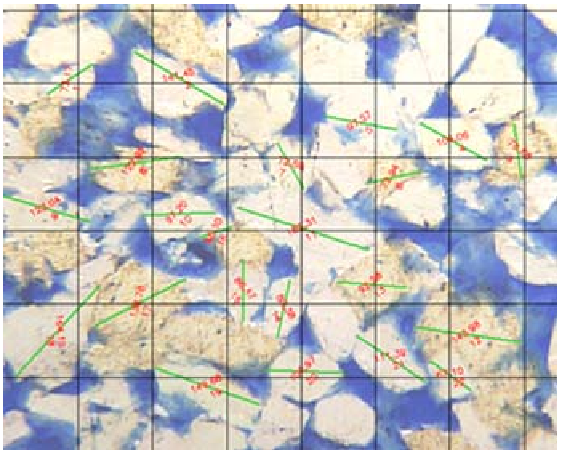

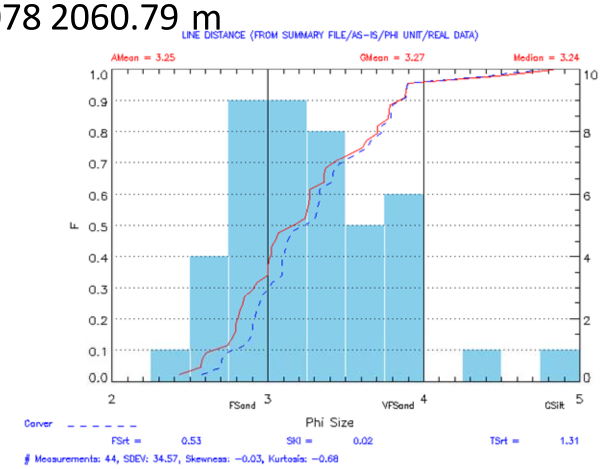

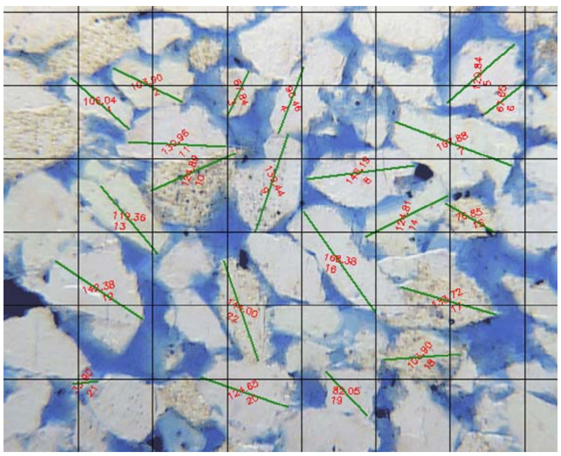

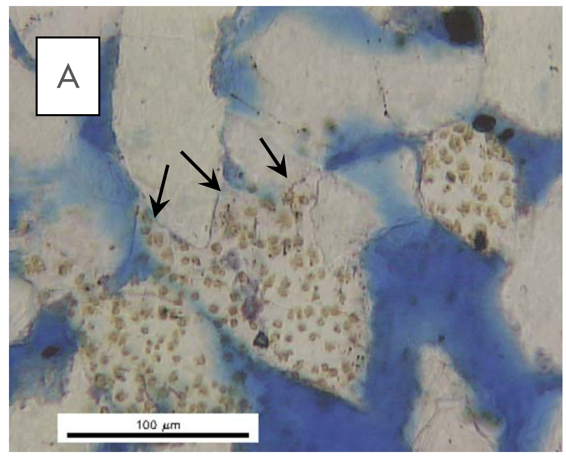

Grain size analysis for the two analyzed images is shown; the summary size distribution plot is shown at upper right. Mean size is 3.25 phi (upper very fine sand) and Trask sorting is 1.31 (moderately well sorted). Black arrows in image A indicate potassium feldspar overgrowths, the dominant feldspar cement observed in this sample.

Radway 072 2060.79 m Post-Test Uniax

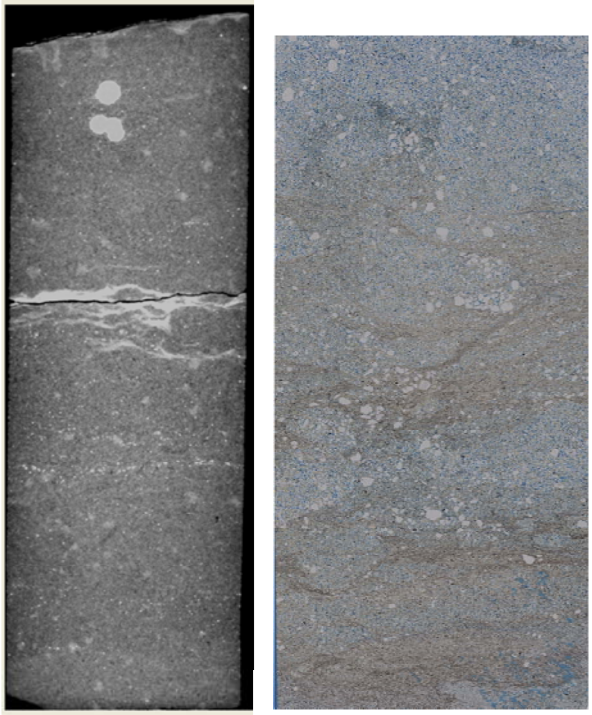

Gray scale image of CT scan of plug RAD072 (left) and transmitted light scan of companion thin section (middle).

Image A shows higher magnification view of a low porosity region in the sample marked by significant volumes of micaceous grains (biotite; green arrows). Image B shows a more porous region. Mean grain size is significantly finer, and sorting significantly better than in deeper units. Mixing of micaceous and nonmicaceous lamina suggests bioturbation.

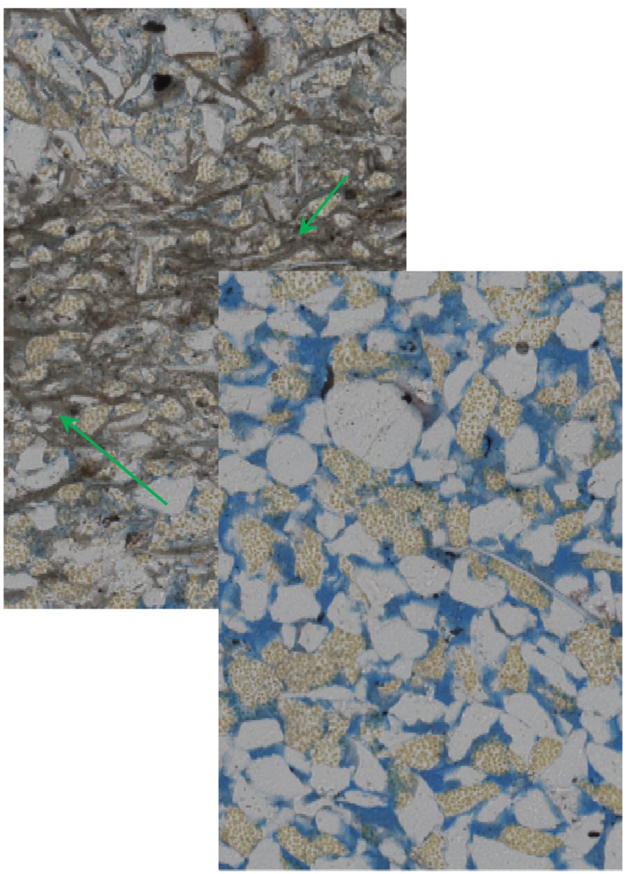

Radway 072 2060.79 m

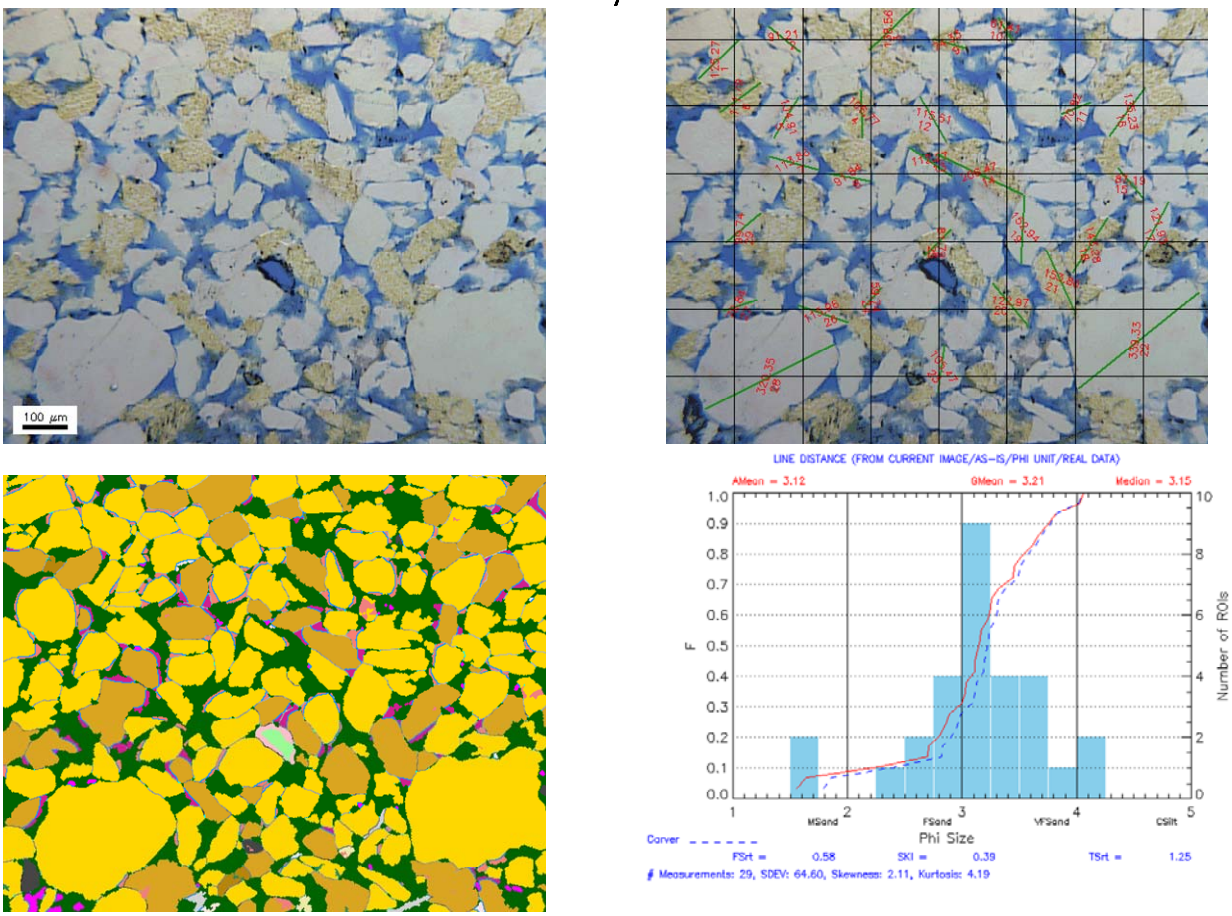

Transmitted light images of plug RAD072 and companion CAP analysis. Mean size is 3.2 phi (upper very fine sand) and Trask sorting is 1.25 (moderately well sorted). Thin section porosity is 20.7% (compare to measured plug porosity of 18.8%). Note that only high porosity (non micaceous) portions of the sample were analyzed. This accounts for the discrepancy between thin section and plug porosity.

A1.3 Zone C (Set 2): 2050 m

The sand at 2050 m is the most poorly sorted and lowest porosity sand in the data set. Mean grain size ranges from 2.1-1.7 phi (upper fine to lower medium sand), and Trask sorting ranges from 1.4-2.1 (moderately to poorly sorted). Discontinuous, biotite rich lamina are common and these, together with the poor sorting in the cleaner layers, result in the low porosity observed in this unit (12.5-13.1% in thin section, and 8.2-11.4% measured on a plug scale). Mineralogically the unit is intermediate between the other two sands examined, with a subarkosic modal composition. Similar to the deepest unit, feldspar tends to be concentrated in finer grained lamina and in the finer grains in poorly sorted intervals. Authigenic cements observed in this interval are predominantly quartz overgrowth (averaging nearly 2% of the whole rock volume), and local pore filling dolomite and anhydrite. Trace volumes of albite overgrowth cement are present on K-feldspar framework grains. This interval is typically the fastest acoustically, consistent with its poorer sorting (lower porosity) and greater degree of cementation. Intergranular volumes observed in this unit range from 16-18%, consistent with the presence of ductile grains and overall poor sorting.

Radway 054 2050.32 m Post-Test In Situ Triax

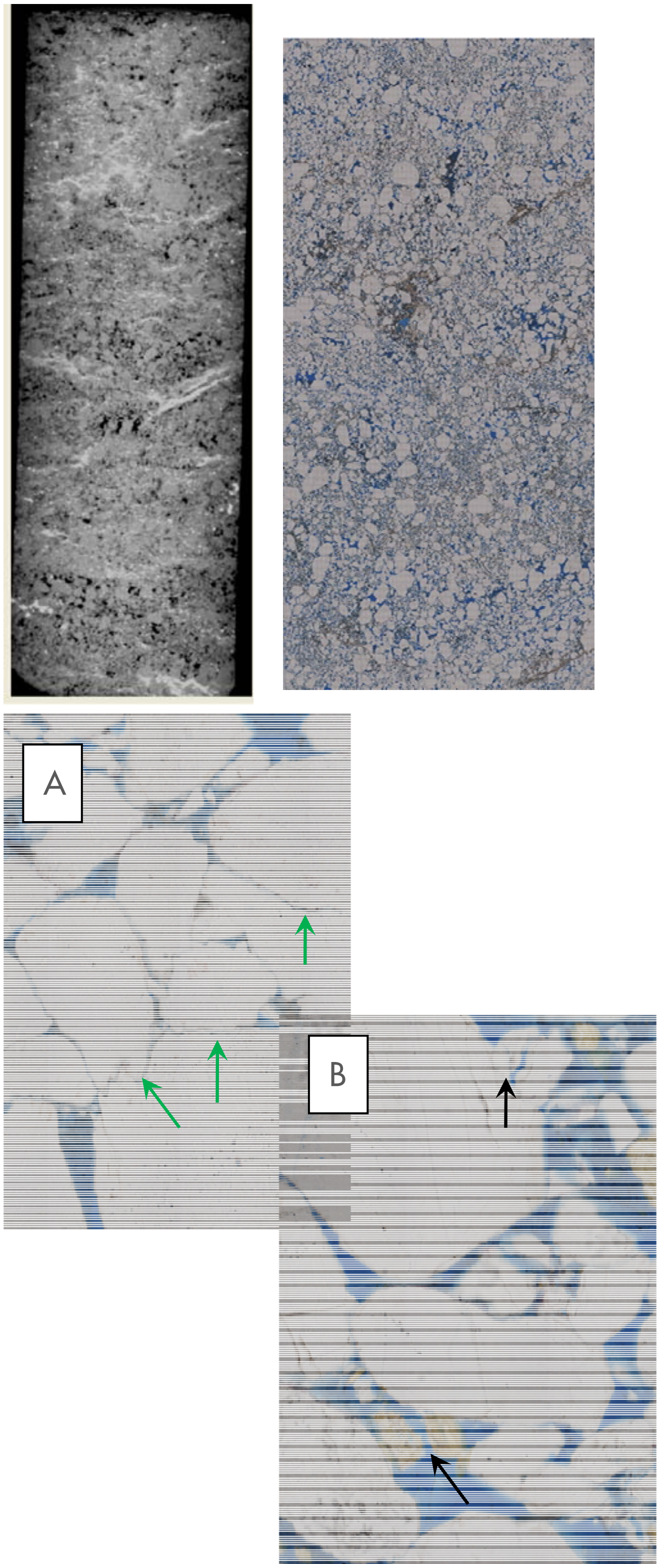

Gray scale image of CT scan of plug RAD054 (left) and transmitted light scan of companion thin section (middle). Image A shows higher magnification view of a low porosity region in the sample marked by significant intergranular pressure solution (green arrows). Image B shows a more porous region. Note that grain fracture is common (black arrows). Similar to RAD055 below, high density regions in the scan are characterized by the presence of detrital biotite.

Radway 054 2050.32 m

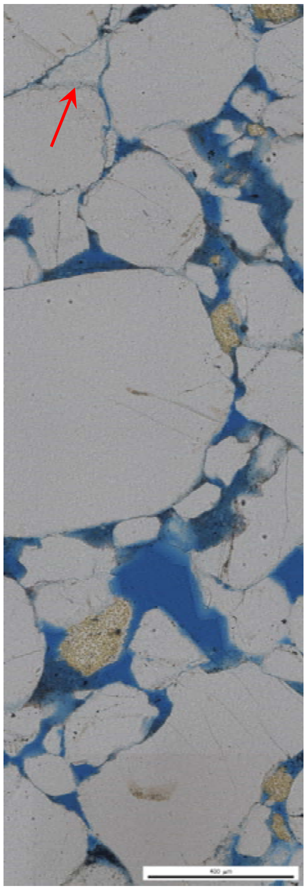

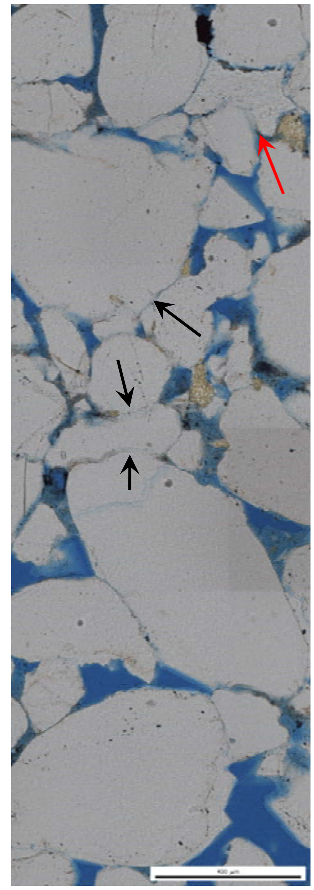

Transmitted light images of plug RAD054 and companion CAP analysis (note that the images are taken from adjacent fields of view and so interpreted image is shown as a single image). Note that only the coarse grained component is represented in this analysis. Dolomite cement is present in the upper portion of both images (red arrows) and post dates quartz overgrowth precipitation, at least in part. Sutured contacts between quartz grains are common (black arrows). Thin section porosity is 12.5%.

Radway 054 2050.32 m

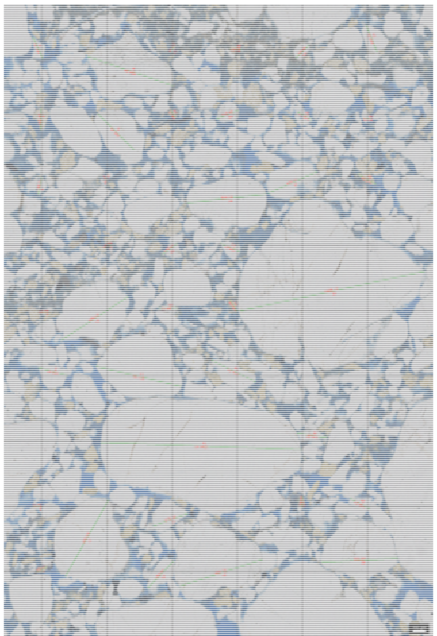

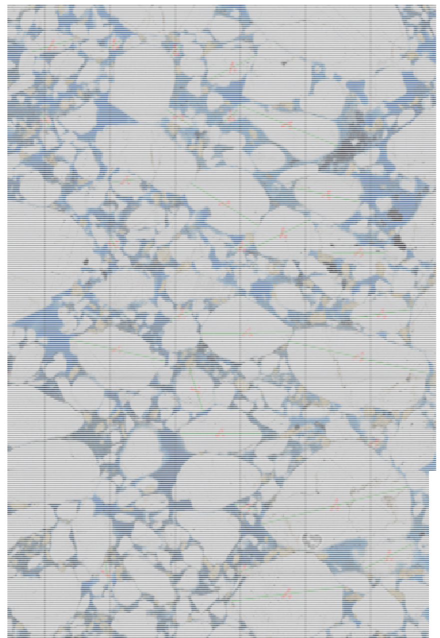

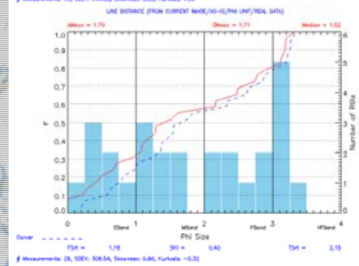

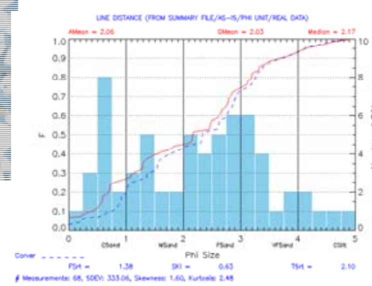

Grain size analysis for the two analyzed images is shown; the summary size distribution plot is shown at the bottom. Mean size is 2.05 phi (lower medium sand) and Trask sorting is 2.10 (poorly sorted).

Radway 055 2050.39 m Post-test Uniax

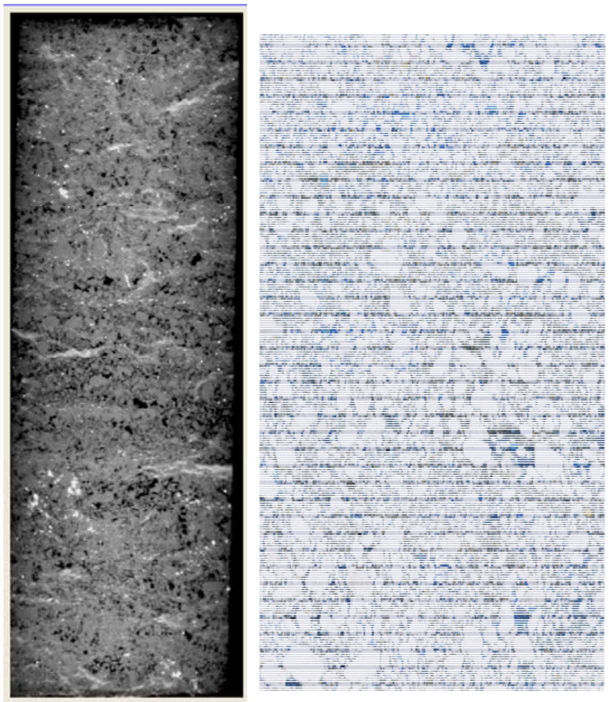

Gray scale image of CT scan of plug RAD055 (left) and transmitted light scan of companion thin section (middle). Image A shows a higher magnification view of a high density region in the scan (matrix supported/biotite rich regions). Image B shows an area where remnant anhydrite cement is observed (black arrow). Note that anhydrite post dates quartz cement precipitation . Red arrow indicates where quartz overgrowth predates anhydrite cement.

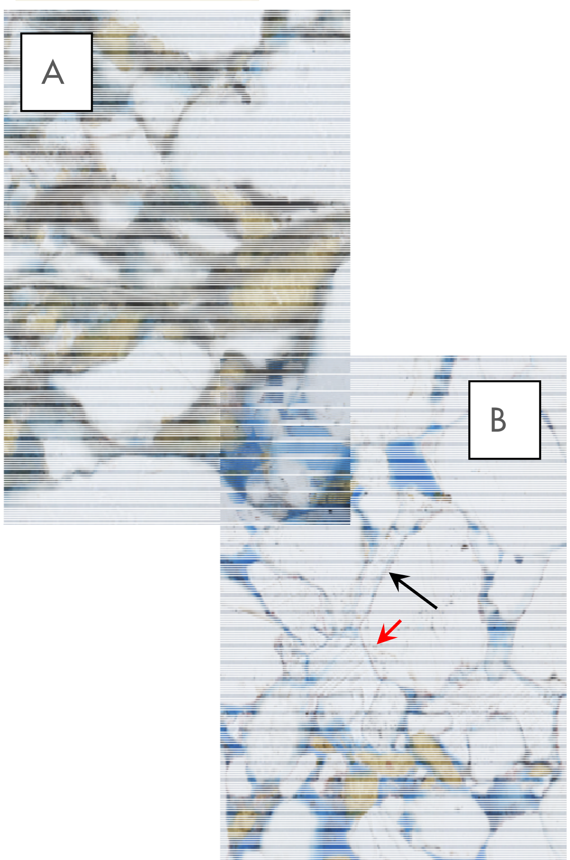

Radway 055 2050.39 m

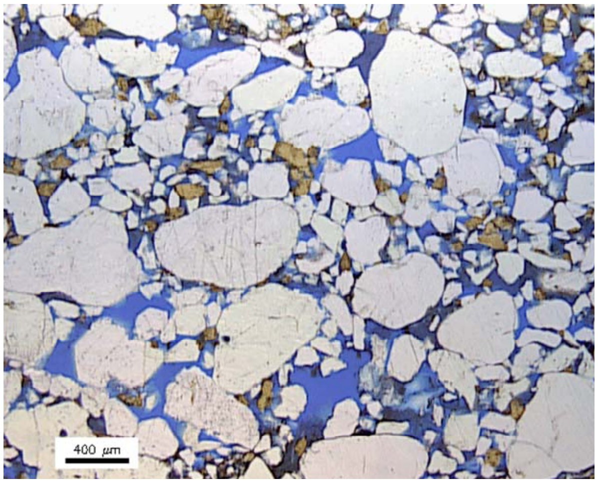

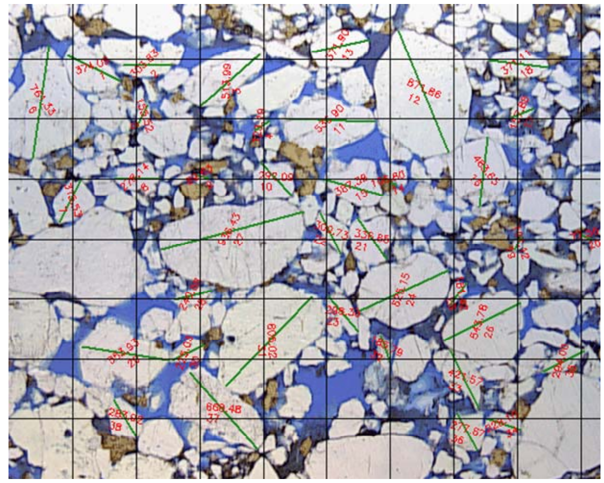

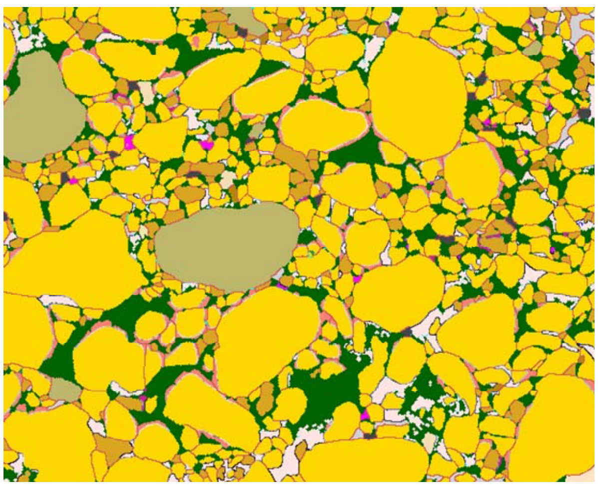

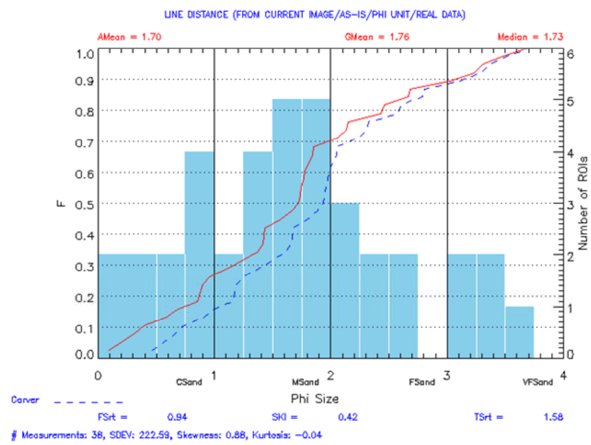

Transmitted light images of plug RAD055 and companion CAP analysis. Note the highly variable texture present on a thin section scale. Potassium feldspar grains are typically finer grained than associated quartz grains. Mean size is 1.7 phi (lower medium sand) and Trask sorting is 1.6 (moderately poor). Thin section porosity is 13.1% (compared to the measured plug porosity of 11.4%).

Radway 055 2050.39 m

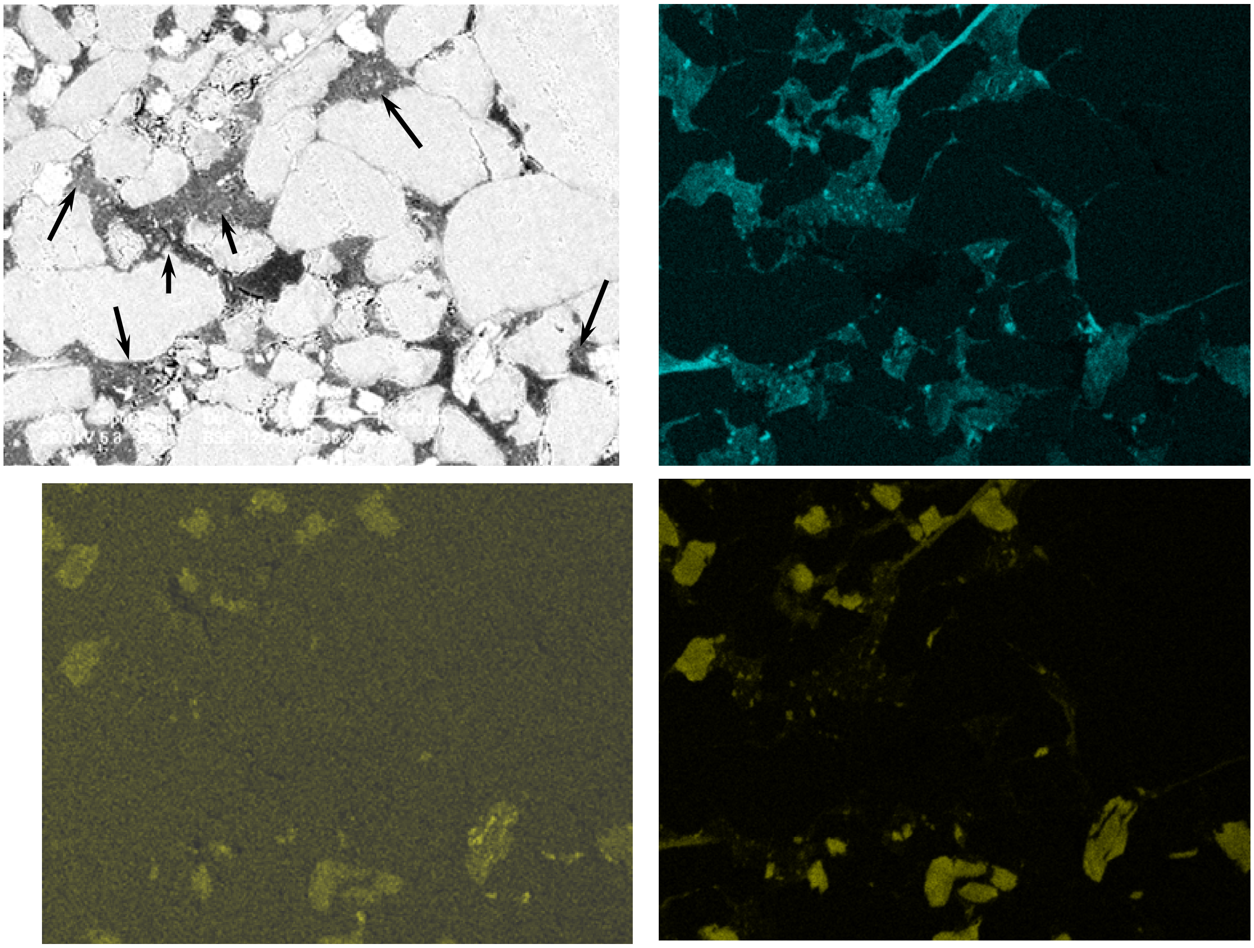

Backscattered electron image of plug RAD055 and major element X-ray dot maps of the same field of view. Map above right shows the distribution of aluminum, and map at lower right shows the distribution of potassium associated with K-feldspar and mica grains in this field of view. Map at lower left shows the distribution of sodium. Note that significant aluminum and potassium are associated with pore filling clay indicated by black arrows in the BSEM image.

Radway 055 2050.39 m

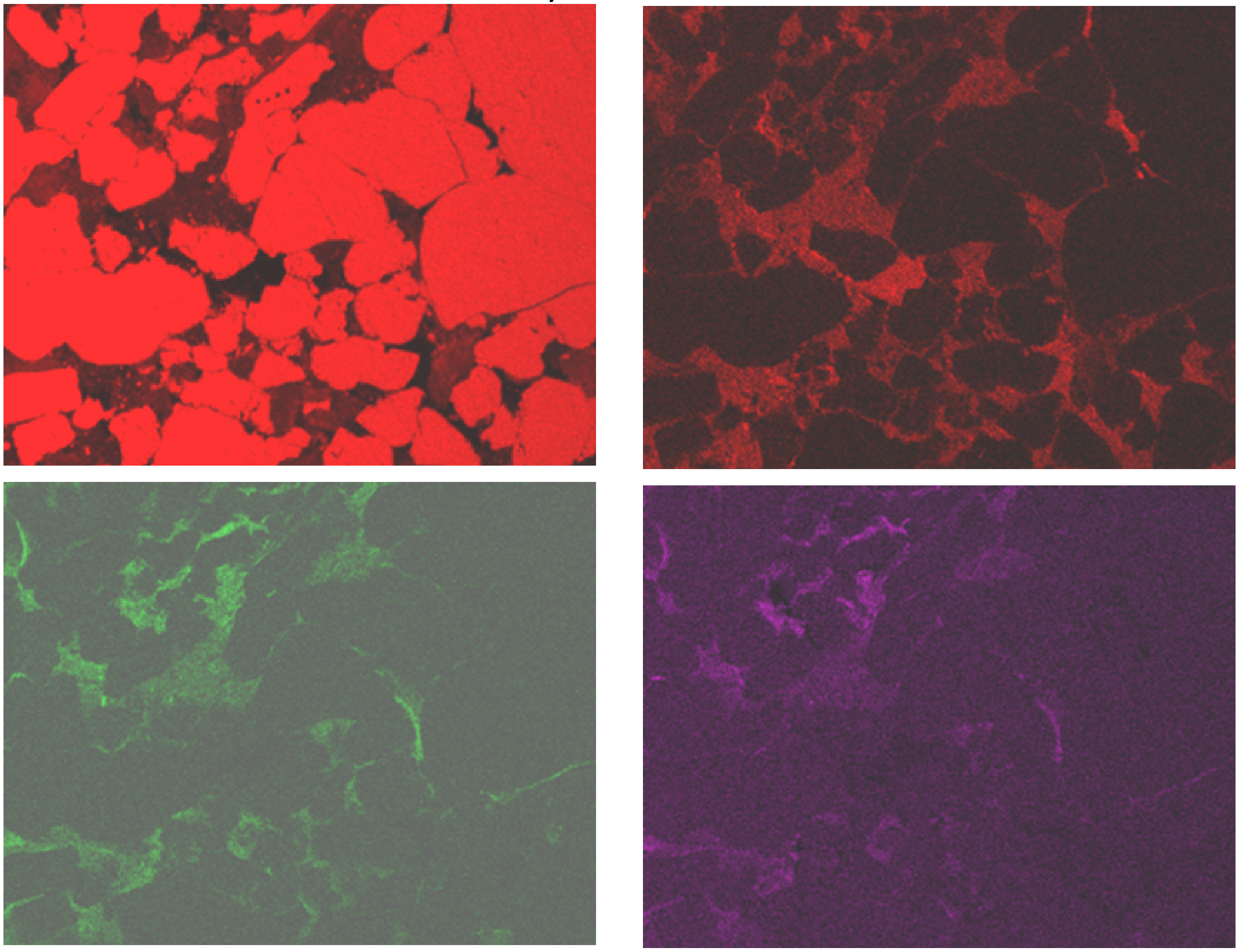

X-ray dot maps showing the distribution of silicon (above left) and carbon (above right). Silicon is present in quartz framework grains and overgrowth cements (bright red) and to a lesser extent in feldspar grains (dull red) and dispersed clay minerals in intergranular space. The carbon response is associated with the epoxy that the sample is impregnated with and thus gives an indication of porosity distribution. Maps at lower left and lower right are the iron and magnesium response respectively. The co-occurrence of Si/Al/K/Fe/Mg is associated with dispersed detrital clay in the sample.

Radway 055 2050.39 m

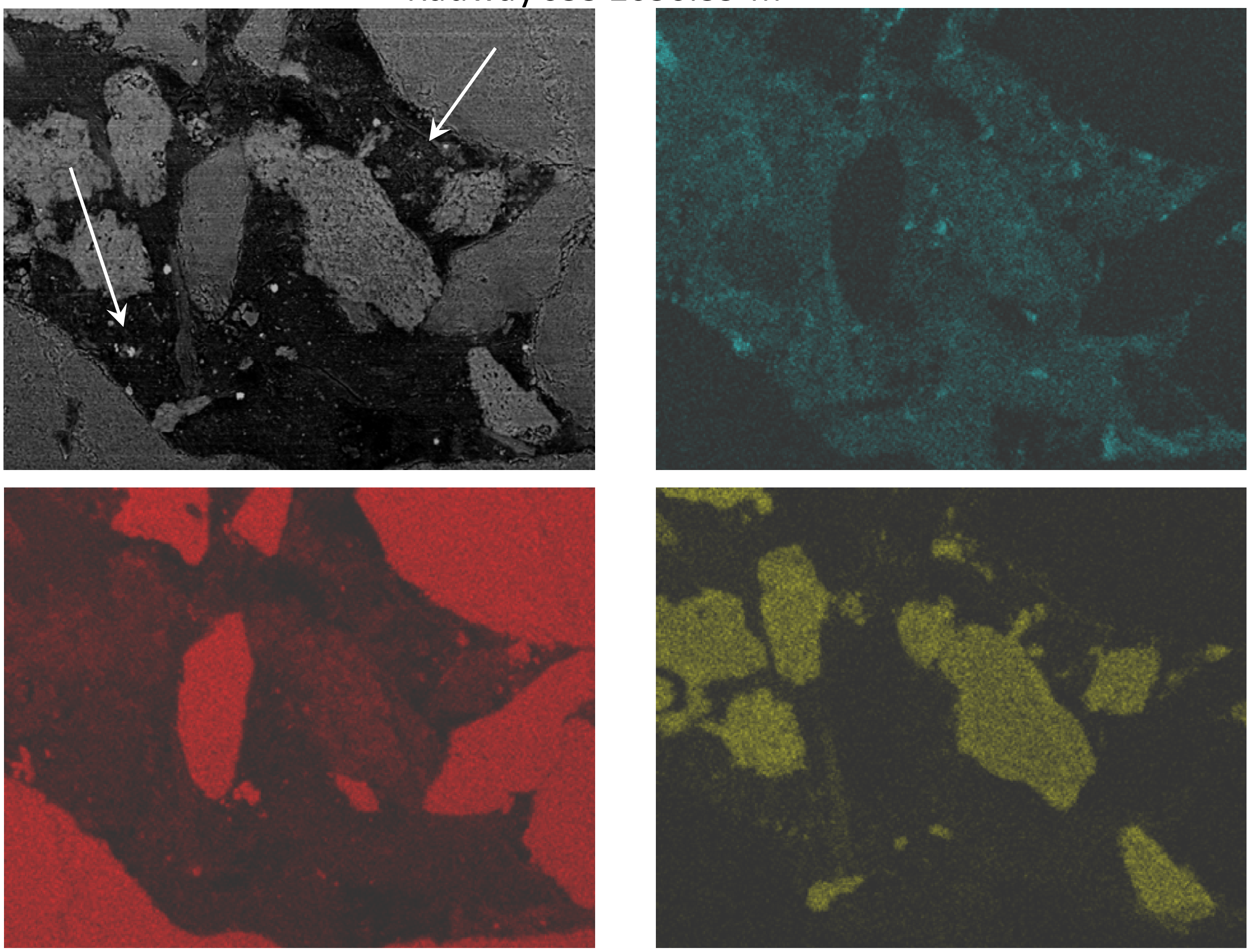

Backscattered electron image of plug RAD055 and major element X-ray dot maps of the same field of view. Map above right shows the distribution of aluminum, and map at lower right shows the distribution of potassium associated with K-feldspar grains in this field of view. Map at lower left shows the distribution of silicon. Note that significant aluminum and potassium are associated with pore filling clay indicated by white arrows in the BSEM image.

APPENDIX 2. DETAILED TEST DATA SUMMARY DVD

The DVD in this appendix contains the digital data summary of the samples and tests reported here. Geomechanical test results are grouped in 7 Excel files in the root directory:

File	**Contents**
BCS_ReportTables.xlsx	Report tables not included in other files
BCSisotropic.xlsx	Isotropic compression test summaries
BCSthermalexp.xlsx	Thermal expansion test summaries
BCStriax2050.xlsx	Triaxial compression zone 2050 m test summaries
BCStriax2061.xlsx	Triaxial compression zone 2061 m test summaries
BCStriax2076.xlsx	Triaxial compression zone 2076 m test summaries
BCSthermalexp.xlsx	Thermal expansion test summaries
BCSuniax.xlsx	Uniaxial compaction test summaries

In addition, there are folders containing CT scans and photographs of the measured plugs and thin section images.